A&A 440, 121–137 (2005)
DOI: 10.1051/0004-6361:20042597

Astronomy & Astrophysics

VLT *K*-band spectroscopy of massive stars deeply embedded in IRAS sources with UCHII colours⋆,⋆⋆

A. Bik[1,2], L. Kaper[1], M. M. Hanson[3], and M. Smits[1]

[1] Astronomical Institute "Anton Pannekoek", University of Amsterdam, Kruislaan 403, 1098 SJ Amsterdam, The Netherlands
e-mail: abik@eso.org
[2] European Southern Observatory, Karl-Schwarzschild Strasse 2, 85748 Garching-bei-München, Germany
[3] University of Cincinnati, Cincinnati, OH 45221-0011, USA

Received 22 December 2004 / Accepted 18 March 2005

Abstract. We have obtained high resolution (R = 10 000) K-band spectra of candidate young massive stars deeply embedded in (ultra-) compact H II regions (UCHIIs). These objects were selected from a near-infrared survey of 44 fields centered on IRAS sources with UCHII colours. Often, the near-infrared counterpart of the IRAS source is a young embedded cluster hosting massive stars. In these clusters, three types of objects are identified. The first type (38 objects) consists of "naked" OB stars whose K-band spectra are dominated by photospheric emission. We classify the K-band spectra of the OB-type cluster members using near-infrared classification criteria. A few of them have a very early (O3-O4 V) spectral type, consistent with a young age of the embedded clusters. The spectral classification provides an important constraint on the distance to the embedded cluster. The ionising power of the population thus derived is compared to the information obtained from the infrared and radio flux of these sources. In most cases these two different determinations of the ionising flux are consistent, from which we conclude that we have identified the ionising star(s) in about 50% of the embedded clusters. The second type (7 objects) are point sources associated with UCHII radio emission, that exhibit nebular emission lines in the near-infrared. Six of the objects in this group produce He I emission indicative of an embedded O-type star. These objects are more embedded than the OB stars and probably do not dominate the infrared flux as measured by IRAS. They may emit the bulk of their reprocessed UV radiation at mm wavelengths. The third type (20 objects) is characterised by broad (100−200 km s^{-1}) Brγ emission and no photospheric absorption profiles. Bik et al. (2005, A&A, submitted) show that these objects are massive YSO candidates surrounded by dense circumstellar disks.

Key words. stars: early-type – stars: formation – stars: distances – ISM: HII regions – infrared: stars

1. Introduction

The recent advent of high-quality, near-infrared instrumentation has opened up a new window on the birth sites of massive stars. The formation timescale of a massive star ($\geq$10 $M_\odot$) is short, of the order of 10 000 yr, so that newly formed stars are still deeply embedded inside their parental molecular cloud.

Observational evidence indicates that at this early stage in the evolution the "hot core" contains an extended circumstellar disk (size ~ 1000 AU; e.g., Beltrán et al. 2004; Chini et al. 2004) through which a vast amount of material would be able to lose its angular momentum and accrete onto the protostar. Before arriving on the main sequence, the young massive star already will produce a strong UV radiation field, ionising its surroundings. At this stage the object will become detectable at far-infrared and radio wavelengths through the heated dust and recombination of hydrogen in the expanding hyper- or ultra-compact H II region (e.g. Churchwell 2002). The same UV radiation field will impact on the extended circumstellar disk and start to destroy it (Hollenbach et al. 1994). The disk destruction timescale is short too (~100 000 yr), so that it becomes an observational challenge to detect and measure any remnants of the formation process of massive stars.

At near-infrared wavelengths one is able to penetrate the obscuring gas and dust in the natal cloud and may detect the photospheric and circumstellar emission of the young massive star. We have carried out an extensive near-infrared survey of fields centered on IRAS sources with the characteristic colours of ultra-compact H II regions (UCHIIs, Wood & Churchwell 1989a) with SOFI on the ESO *New Technology Telescope* (Kaper et al. 2005).

The main result in this survey is that in all 44 regions but one a near-infrared source associated with Brγemission is found. In 75% of the fields this near-infrared emission corresponds to an embedded massive stellar cluster

⋆ Based on observations collected at the European Southern Observatory at La Silla and Paranal, Chile (ESO programs 64.H-0425 and 65.H-0602).
⋆⋆ Table 6 is only available in electronic form at http://www.edpsciences.org

($A_V \sim 10-20$ mag). Only a small fraction of the near-infrared sources have a size typical of UCHII regions i.e. 0.1 pc. Besides the embedded clusters, we have detected the near-infrared counterpart of a dozen ultra-compact radio sources (i.e. in 40% of the fields in which an ultra-compact radio source is located).

This paper concentrates on the spectroscopic follow-up of the sources selected from our near-infrared NTT survey to confirm their massive-star nature and to search for observational signatures that may reveal information on the formation process. K-band spectra have been obtained of candidate young massive stars identified in our survey with ISAAC mounted on the ESO *Very Large Telescope*, based on their K-band magnitude and $J-K$ colour. These candidate massive stars are members of the embedded cluster or, in some cases, the potential ionising stars of UCHIIs.

The K-band window is well suited to perform the spectral classification of OB-type stars (Hanson et al. 1996), especially when interstellar extinction becomes important. However, in order to retrieve the photospheric spectrum of an embedded massive star, one has to correct for the strong nebular emission produced by the surrounding H II region. As OB-type stars mainly include lines of hydrogen and helium in their spectra, many photospheric lines will be affected by nebular emission. When using ISAAC with a 0.3 arcsec slit, the spectral resolution ($R \simeq 10\,000$) becomes sufficient to resolve the broad photospheric lines and to discriminate between the nebular and stellar contribution. The feasibility of this approach has been demonstrated by Watson & Hanson (1997) who retrieved the photospheric spectrum of the O5–O6.5 V star ionising the famous cometary UCHII G29.96-0.02 (see also Martín-Hernández et al. 2003). In the mean time the photospheric spectra have been registered of massive stars embedded in a handful of UCHIIs (e.g. Hanson et al. 2002).

Through the direct measurement of the spectral properties of the deeply embedded, young massive stars, a comparison can be made with estimates based on the far-infrared and radio emission produced by the UCHII c.q. embedded cluster. Following this procedure, Bik et al. (2003) were able to identify the long-sought-for ionising star of the Flame Nebula (NGC 2024). As a by-product of the spectral classification, the amount of interstellar extinction A_V can be determined as the intrinsic $J-K$ colour of OB stars falls within a narrow range. A relation between spectral type and luminosity then helps to constrain the distance to the embedded cluster, providing important information on the distribution of the embedded massive star population in the Milky Way. Furthermore, one can investigate whether these young massive stars differ from the OB-star field population, e.g. with respect to their wind and rotation properties, and whether they show any signs that reveal information on the formation process.

The paper is organised as follows; the next section describes the VLT/ISAAC spectroscopic observations and the applied data reduction procedure. In Sect. 3 we introduce the K-band spectra and divide them into different classes. We also outline the spectral classification method. Using the spectroscopic parallax, the distances to the OB stars are estimated and compared to literature values. Section 4 includes the K-band spectra of the near-infrared counterparts of the UCHII regions detected at radio frequencies. In Sect. 5 the luminosity of the OB star population thus identified is compared to that inferred from the infrared and radio measurements. Section 6 discusses the properties of the young OB stars with respect to those measured in the field population. The last section summarises our conclusions.

2. Observations

K-band spectra were taken of point sources in 31 regions from the sample of 44 IRAS sources with UCHII colours presented in Kaper et al. (2005). The point sources were selected based on their position in the colour-magnitude diagram. The brightest and most reddened sources were selected for follow-up spectroscopy.

Medium-resolution, long-slit (120″) K-band spectra were obtained with ISAAC mounted on Antu (UT1) of ESO's *Very Large Telescope* (VLT), Paranal, Chile. The observed targets and the observing log are given in Table 6. The observations were carried out during a visitor mode run (by LK and MMH) on March 18–20, 2000, and a service mode run in the period between May 18 and July 16, 2000. A slit width of 0.3″ was used, resulting in a spectral resolving power $R = 10\,000$. The slit position was chosen such that at least two sources were positioned on the slit. The observing conditions at Paranal Observatory were excellent: humidity less than 10% and seeing ranging from 0.5–1.0″.

The central wavelength was chosen such that the most important lines needed to classify the OB stars in the K-band are covered (see Sect. 3.1). The spectra taken in visitor mode (the objects with RA between 5 and 15 h) have a central wavelength of 2.129 μm and range from 2.069 to 2.189 μm. This setting should have covered the He II line at 2.1885 μm; it turned out, however, that the last 20 pixels were vignetted and not usable. In the service mode run (sources with RA between 16 and 19 h) the central wavelength was shifted to 2.134 μm in order to cover the He II line.

The electrical ghosts and bias were removed from the frames before flatfielding. Despite the use of flatfields taken during the night, some service mode flatfields have a fringe pattern different from that of the science frames and thus introduce fringes in the final spectrum. These flatfields were not used and replaced by flatfields obtained in other nights which cause less fringing; in some spectra, however, remnants of fringes are still visible. The wavelength calibration of the spectra is performed using arc spectra with the IRAF task *identify*. The typical error of the wavelength solution is 3 km s^{-1}.

In order to correct for the sky background, the object was "nodded" between two positions on the slit (A and B) such that the background emission registered at position B (when the source is at position A) is subtracted from the source plus sky background observation at position B in the next frame, and vice versa. The offsets were such that the two stars positioned on the slit are not overlapping. In some sources, the nebular lines (e.g. Brγ) are spatially extended and will overlap resulting in artifacts in the sky subtracted image. This can mimic a narrow absorption feature superimposed on the stellar Brγ line.

Telluric absorption lines were removed using stars of spectral type B8V – A2V, observed under identical sky conditions. Before removing the telluric lines, the only photospheric line (Brγ) in the spectrum of the A star needs to be divided out. It turns out that the best result is achieved when first the telluric features are removed from the *K*-band spectrum of the telluric standard using a high-resolution telluric spectrum (obtained at NSO/Kitt Peak). This spectrum is taken under very different sky conditions, so numerous spectral remnants remain visible in the corrected standard star spectrum. Without this "first-order" telluric-line correction, a proper fit of Brγ cannot be obtained. The Brγ line is fitted by a combination of two exponential functions. The error on the resulting Brγ equivalent width (*EW*) of our target star is about 5%. After the removal of the Brγ line of the A star, the telluric lines are removed by taking the ratio of the target spectrum and the telluric spectrum. This is done using the IRAF task *telluric*, which allows for a shift in wavelength and a scaling in line strength, yielding a more accurate fit. The task uses a cross-correlation procedure to determine the optimal shift in wavelength and the scaling factor in line strength, which can be changed interactively. The shifts are usually a few tenths of a pixel; also the scaling factors are modest (∼10%).

3. *K*-band spectra of young OB stars

The *K*-band spectra can be divided in different classes (see Fig. 1 for an example of the different spectra). Forty objects turn out to be late-type (fore- or background) stars, with *K*-band spectra dominated by many absorption lines (Fig. 1e). These stars are a natural by-product of our selection criteria. They emit the bulk of their radiation in the (near) infrared and have a red intrinsic colour. The other three classes are different types of objects connected with star-forming regions.

Thirty-eight objects show the spectral features indicative of OB stars and are the subject of this study (Figs. 1a,b). In the following, we will describe the classification method introduced by Hanson et al. (1996). The spectra are presented and classified, distances are estimated based on the *K*-band spectral type (spectroscopic parallax). The second type of objects discussed in this paper are the near-infrared counterparts of the UCHII regions with nebular *K*-band spectra (Fig. 1c).

Another 20 objects show broad, spectrally resolved Brγ emission (Fig. 1d) and are presented in Bik et al. (2005). These emission-line objects are classified as massive Young Stellar Objects (YSOs). Towards some of these objects CO first-overtone emission is detected, originating from warm (2000−4000 K) and dense (10^{10} cm^{-3}) material. Bik & Thi (2004) show that the CO emission in these objects is coming from a Keplerian rotating disk within 5 AU from the central star. These objects are very likely surrounded by the remnant of a accretion disk. Photo-evaporation models show that the outer parts of the accretion disk get photo-evaporated on a very short timescale, while the inner parts of the disk remain present around the recently formed star for a longer time (Hollenbach et al. 1994).

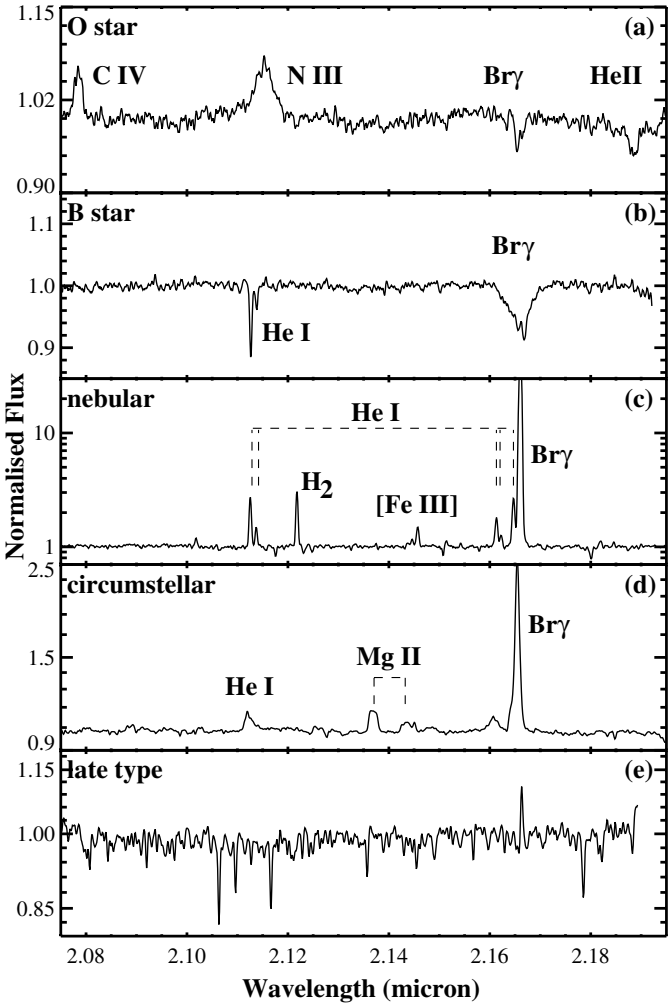

Fig. 1. *K*-band spectra of the different classes of objects found in our spectroscopic survey. Panels **a)** and **b)** show the photospheric *K*-band spectra of O and B stars which is the main focus of this paper. Panel **c)** shows a spectrum dominated by nebular emission from the UCHII region. The emission lines are narrow and not resolved. This in contrast to the spectrum displayed in panel **d)** where the emission lines are resolved. This object shows characteristics of a massive YSO. Panel **e)** displays a spectrum of a late type (fore-/background) star. The spectrum is dominated by absorption lines. The narrow Brγ emission line originates in the H II region. Note that panels **c)** and **d)** are plotted on a logaritmic scale.

3.1. Classification scheme

Hanson et al. (1996) constructed a *K*-band classification scheme based on the relative line strength in spectra of OB stars with known (optical) MK spectral type. The stars were independently classified, and the derived *K*-band classes compared with MK spectral types.

The lines covered by the *K*-band spectra of massive stars are a hydrogen line (Brγ 2.16 μm), three He I lines, one at 2.058 μm (not in our spectral setting), and two at 2.112 and 2.113 μm. Also a He II line is present at 2.185 μm. The other lines detected in O star spectra are a complex of N III lines at 2.115 μm and three C IV lines with the two strongest at 2.069 and 2.078 μm and a very weak line at 2.083 μm.

Table 1. Spectral classification of OB stars as proposed by Hanson et al. (1996). *abs*: in absorption, *em*: in emission, *w*: weak, *np*: not present. For the lines not detected in the low-resolution spectra, upper limits are used; for N III: 0.2 Å and for the other lines 0.3 Å is used as upper limit. For the Brγ criterium, between brackets the modification as discussed in the text is indicated. The K-band spectral type (Col. 1) is based on the presence of the lines listed in this table and is derived independently of the corresponding MK spectral type. In the K-band spectra of early-O stars the N III and C IV lines are important diagnostics. At late-O the He I line starts to become important, while for B stars, the main diagnostic is the strength of the Brγ line.

K-band Spec. type	MK Spec. type	C IV 2.078 μm (Å)	N III 2.115 μm (Å)	He I 2.113 μm (Å)	H I(Brγ) 2.166 μm (Å)	He II 2.185 μm (Å)
Dwarfs and Giants						
kO3–O4	O3V–O4V	np	em	np	≤4(5)	abs
kO5–O6	O5V–O6.5V	em	em	np	≤4(5)	abs
kO7–O8	O7V–O8V	w/np	em	abs	≤4(5)	w, abs
kO9–B1	O8V–B1V	np	np	abs	≤4(5)	np
kB2–B3	B1V–B2.5V	np	np	abs	4(5) − 8	np
kB4–B7	B3V–B7V	np	np	np	4(5) − 8	np
kB8–A3	B8V–A3V	np	np	np	>8	np
Supergiants						
kO3–O4b	O3I–O4I	np	np	np	w/em	em, abs
kO5–O6b	O5I–O6.5I	em	em	np	w/em	abs
kO7–O8b	O7I–O8I	w/np	em	abs	w/em	w, abs
kOBb	O9I–B3I	np	np	abs	em	np

The Brγ line is present in both the O and B type stars, and increasing in strength from the early O toward late B/early A. The He II line strength is decreasing toward later spectral type and the line disappears when the spectral type becomes later than O7/O8. The C IV (emission) lines are only visible for a small range in effective temperature. Hanson et al. (1996) find that stars with spectral type between O5 and O6.5, and down to O8 in supergiants, have C IV lines in their spectrum, making it a sensitive temperature diagnostic. The identification of the emission complex at 2.1155 micron is still uncertain, but is assumed to be N III. The line is visible in stars with spectral type between O3 and O8. The He I lines at 2.112/2.113 μm start to become visible in O7-O8 stars and remain present till B3 in dwarfs and as late as B8 or B9 in supergiants.

The classification scheme developed by Hanson et al. (1996) is summarised in Table 1. The classification of OB stars in the K-band is hampered by the limited number of lines as well as the few spectra available. The K-band classification is therefore not as accurate as the optical classification. Especially for the B stars, where only two lines are present (He I and Brγ), the classification becomes less reliable.

As the spectral resolution and signal-to-noise ratio of the spectra presented in this paper are different from the data used by Hanson et al. (1996), care should be taken in applying the classification of Hanson et al. (1996) right away. To be able to compare our observations with the low-resolution spectra of Hanson et al. (1996) we observed spectra of optically visible OB stars with VLT/ISAAC. The optically visible OB stars are located in the Tr 16 cluster in the Car OB2 association (Thé et al. 1980) and NGC 6231 in the Sco OB1 association (Sung et al. 1998). The spectra are shown in Fig. 2, plotted in order of optical MK-spectral type. The spectra of the O stars in Car OB2 were taken during the visitor mode run, when the He II line was not well covered. In the K-band spectra of the stars in NGC 6231, the He II line is not present as the stars are of later spectral type.

Applying the classification criteria developed by Hanson et al. (1996) to the spectra of the "reference stars" does for some of the stars not result in a classification consistent with their MK spectral type. The spectra of the classification stars in Hanson et al. (1996) have a resolving power varying between $R = 800$ and $R = 1100$, with a few stars taken at a resolution of 3000. While the spectra presented in this paper are taken with a spectral resolution of 10 000 and in the most cases higher signal-to-noise ratio. The difference in spectral resolution and signal-to-noise between our spectra and those used by Hanson et al. (1996) results in slightly different classification criteria.

In a low-resolution spectrum the He I 2.112/2.113 lines are not resolved and are observed as one line. In our spectra, these lines are resolved and can provide information on the shape of the line. The higher spectral resolution and the higher signal-to-noise ratio of our spectra enables the detection of lines with lower EW than could be detected by Hanson et al. (1996). An illustration of this is the presence of the He I line in the spectrum of HD 303311. The star is optically classified as O5V, which, according to classification of Hanson et al. (1996), does not show the He I line in the spectrum. However, the He I line is detected in our high-resolution spectrum. When smoothed to a resolution of $R = 1100$, the He I line disappears. This He I line is also visible in the newly taken higher resolution spectra of O5V-O6V stars (Hanson et al., in prep.). Therefore, upper limits reflecting the smallest EW detected by Hanson et al. (1996)

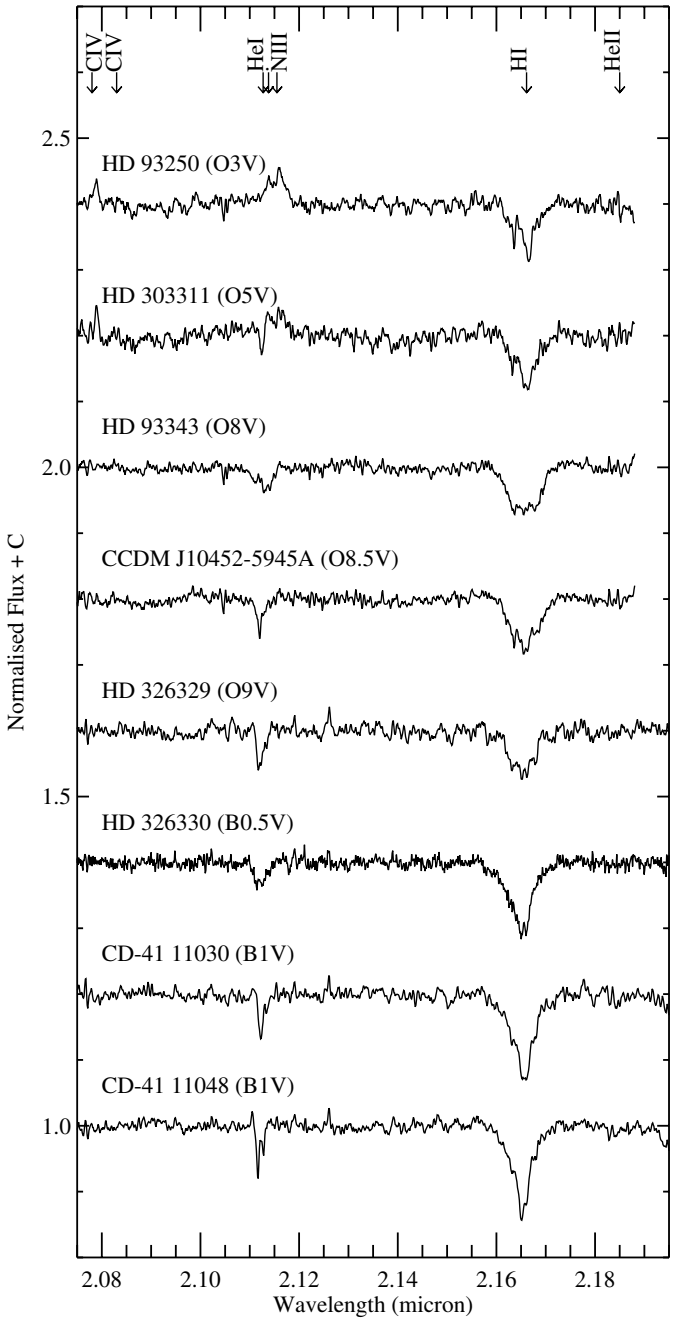

Fig. 2. *K*-band spectra of optically visible OB stars in Tr 16 and NGC 6231. Application of the classification criteria introduced by Hanson et al. (1996) yields spectral types consistent with the MK classification. The higher spectral resolution results in the detection of the He I line in O5 V stars, which is not seen in the low resolution spectra of (Hanson et al. 1996).

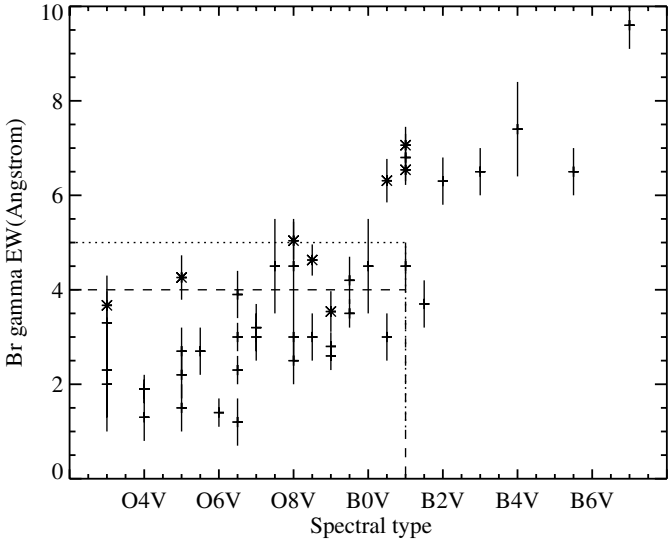

Fig. 3. The *EW* of Brγ plotted versus spectral type. The points represented by the "+" signs are taken from Hanson et al. (1996). The *EW*s indicated with a "$\star$" are from our comparison spectra in Fig. 2 (see also Table 2). The dashed line represents the criterion of 4 Å to discriminate between the kO9–B1 and kB2–B3 spectral classes. However, a lot of O8V–B0V stars have Brγ *EW*s larger than 4 Å and would be wrongly classified as kB2-B3. By shifting the criterion to 5 Å, the O8V–B0V stars would be correctly classified.

are used in the classification scheme for lines that were not detected by Hanson et al. (1996). The *EW* of the He I line in the spectrum of HD 303311 falls below the adopted upper limit for the He I line (0.3 Å).

Another adaptation we applied to the classification scheme of Hanson et al. (1996) is the division between the kO9−B1 and kB2−B3 spectral classes. The difference between the kO9−B1 and kB2−B3 spectral classes is only based on the strength of the Brγ line; for both spectral classes the He I line is of comparable strength. The division between those two classes is set at a Brγ *EW* of 4 Å. A substantial number of O8V–B1V stars, however, have a Brγ *EW* between 4 and 5 Å (Fig. 3): the *EW* of the Brγ line in the O8-O9 stars HD 93343 (O8V), CCDM J10452-5945A (O8.5V) and HD 326329 (O9V) is 5.0, 4.6, and 3.5 respectively. By shifting the division to 5 Å, the O8V-B0V stars are classified as kO9-B1 stars. Ideally, line-ratios are much better suited for spectral classification. However, due to the lack of lines in the late-O and early-B stars, the *EW* of Brγ has to be used. This problem does not occur when discriminating kB2–B3 and kB4–B7 as in between these two spectral classes the He I line disappears.

Hanson et al. (1996) do not find a significant difference in spectral features between the dwarfs (luminosity class V) and the giants (III). The supergiants, however, show a different spectrum, especially in the Brγ and helium lines, where the stronger stellar wind produces emission lines (or wind emission fills in the absorption lines).

3.2. Spectral classification of embedded OB stars

The *K*-band spectra of the embedded OB stars are presented in Figs. 4 and 5. In the remaining part of the paper we will name the objects after the first 5 digits (i.e. the right ascension) of the IRAS point source they are associated with, together with a number based on our photometry (e.g. object 647 in IRAS 19078+0901 we refer to as 19078nr647, cf. Kaper et al. 2005). Two spectra include strong emission lines characteristic of OB supergiants and WR stars (Fig. 6). Because of the presence of photospheric lines, like N III and C IV, these objects were not included in the massive YSO sample (Bik et al. 2005)

Table 2. *EW* measurements and *K*-band classification of the optically visible reference stars in Tr16 and NGC 6231 (Fig. 2). Column 1 gives the name and the spectral type as provided by Simbad. Columns 6 and 7 list the *K*-band spectral type applying the classification scheme of Hanson et al. (1996) and the corresponding optical MK classification.

Object	C IV (Å)	N III (Å)	He I (Å)	H I(Brγ) (Å)	*K*-band Sp.Type	Optical Sp.Type
HD 93250 (O3V)	-0.49 ± 0.1	-2.11 ± 0.35	–	3.67 ± 0.3	KO5–O6	O5V–O6.5V
HD 303311 (O5V)	-0.58 ± 0.1	-1.17 ± 0.4	0.28 ± 0.07	4.26 ± 0.47	KO5–O6	O5V–O6.5V
HD 93343 (O8V)	–	–	1.24 ± 0.27	5.04 ± 0.4	kO9–B1	O8V–B0V/B1V
CCDM J10452-5945A (O8.5V)	–	–	0.82 ± 0.12	4.63 ± 0.33	kO9–B1	O8V–B0V/B1V
HD 326329 (O9V)	–	–	0.94 ± 0.14	3.54 ± 0.43	kO9–B1	O8V–B0V/B1V
HD 32633 (B05V)	–	–	0.99 ± 0.21	6.31 ± 0.46	kB2–B3	B1V–B2.5V
CD-41 11030(B1V)	–	–	0.94 ± 0.11	7.06 ± 0.39	kB2–B3	B1V–B2.5V
CD-41 11048 (B1V)	–	–	0.81 ± 0.10	6.54 ± 0.32	kB2–B3	B1V–B2.5V

even though they show Brγ in emission. The spectra in Figs. 4 and 5 are plotted according to their *K*-band spectral type (see Table 4 and below).

The *EW* measurements are presented in Table 3 in order of right ascension of the IRAS source. In some spectra, the He I and/or the Brγ lines are suffering from nebular contamination. In most of these, the lines have been subtracted out before measuring the He I or Brγ *EW*. In a few cases the nebular He I emission was so strong that the underlying absorption could not be detected any longer (noted in Table 3 as "neb"). This problem was less severe in case of Brγ as the photospheric absorption line is much broader than the nebular emission line. Also the He I nebular lines at 2.161 and 2.165 μm which are sometimes present bluewards of Brγ do not prevent the detection of the broad Brγ absorption. The error on the *EW* is determined taking into account the signal-to-noise ratio of the spectrum (see Col. 5, Table 6) and the peak over continuum ratio of the line.

The *K*-band spectra are classified based on the method outlined in Sect. 3.1. The resulting spectral class and the corresponding range in optical spectral type is given in Cols. 2 and 3 of Table 4. As described in Sect. 3.1, the difference between kO9–B1 and kB2–B3 is only the strength of the Brγ line. An *EW* of 5 Å is used to discriminate between these two spectral types. The spectra where the *EW* measurement of Brγ is equal (within the errors) to 5 Å are classified as kO9−B1/kB2−B3.

In 16177nr405 (Fig. 4, left panel), the Brγ absorption line is not detected. The spectral type derived for this object is based on the presence of the C IV and N III lines. The He I line, if present, could not be detected because of strong nebular emission. For this spectral type (kO5-O6), He II should also be present in the spectrum. The He II line, however, is hardly detected, a little hint of absorption may be present. Also in 18449nr319 (Fig. 4, left panel) the He II line is not detected. Data taken at a second epoch (Apai 2004) indicate that the He II line in the spectrum of 18449nr319 is present. This suggests that an instrumental effect may be responsible for these non-detections. In 16177nr405, however, the He II line is absent in both epochs. The Brγ line in 18507nr262 (Fig. 4, left panel) shows a remarkable profile. The absorption in the center of the line is due to over-subtraction of the spatially extended nebular Brγ emission. The emission wings, however, are real, suggesting that this Brγ line is in emission. The full width at zero intensity (*FWZI*) is ~800 km s^{-1}.

3.3. Emission line objects

The spectra of 17423nr3102 and 18449nr335 clearly show Brγ in emission (Fig. 6). These stars do not share the other spectral properties of massive YSOs, which do show Brγ in emission, but no C IV and N III emission nor He II absorption. In the *K*-band spectrum of 17423nr3102 C IV and N III are present, as well as He II absorption. These lines are formed in the photosphere of the star. Cotera et al. (1999) classify this star as a Be star, based on a low-resolution *K*-band spectrum. This classification can be excluded by our high-resolution spectrum. The *K*-band spectra of Be stars do not show C IV and N III emission lines (Clark & Steele 2000). Applying the classification scheme of Hanson et al. (1996) the source would be classified as kO5-O6b, an O5-O6.5 supergiant.

The *K*-band spectrum of 18449nr335 displays very broad Brγ emission profiles with a triangular shape, characteristic of Wolf-Rayet stars. This star is located in the center of W43 and is classified by Blum et al. (1999) as a WN7 star.

3.4. Distance determinations

The kinematic distance of the UCHII regions is listed in Col. 4 of Table 4. These distances are derived from the radial velocity measurements of the CS(2–1) line (Bronfman et al. 1996). A model for the galactic rotation developed by Brand & Blitz (1993) is used to convert the radial velocity into a distance estimate. For sources located inside the solar-circle, a near and a far distance is given. In Col. 5 of Table 4 the distance adopted in Kaper et al. (2005) is given. These estimates are obtained from the literature and based on, e.g., star counts, radio recombination lines and optical photometry.

These two distance estimates can be compared with the distance derived from the *K*-band spectral type and photometry

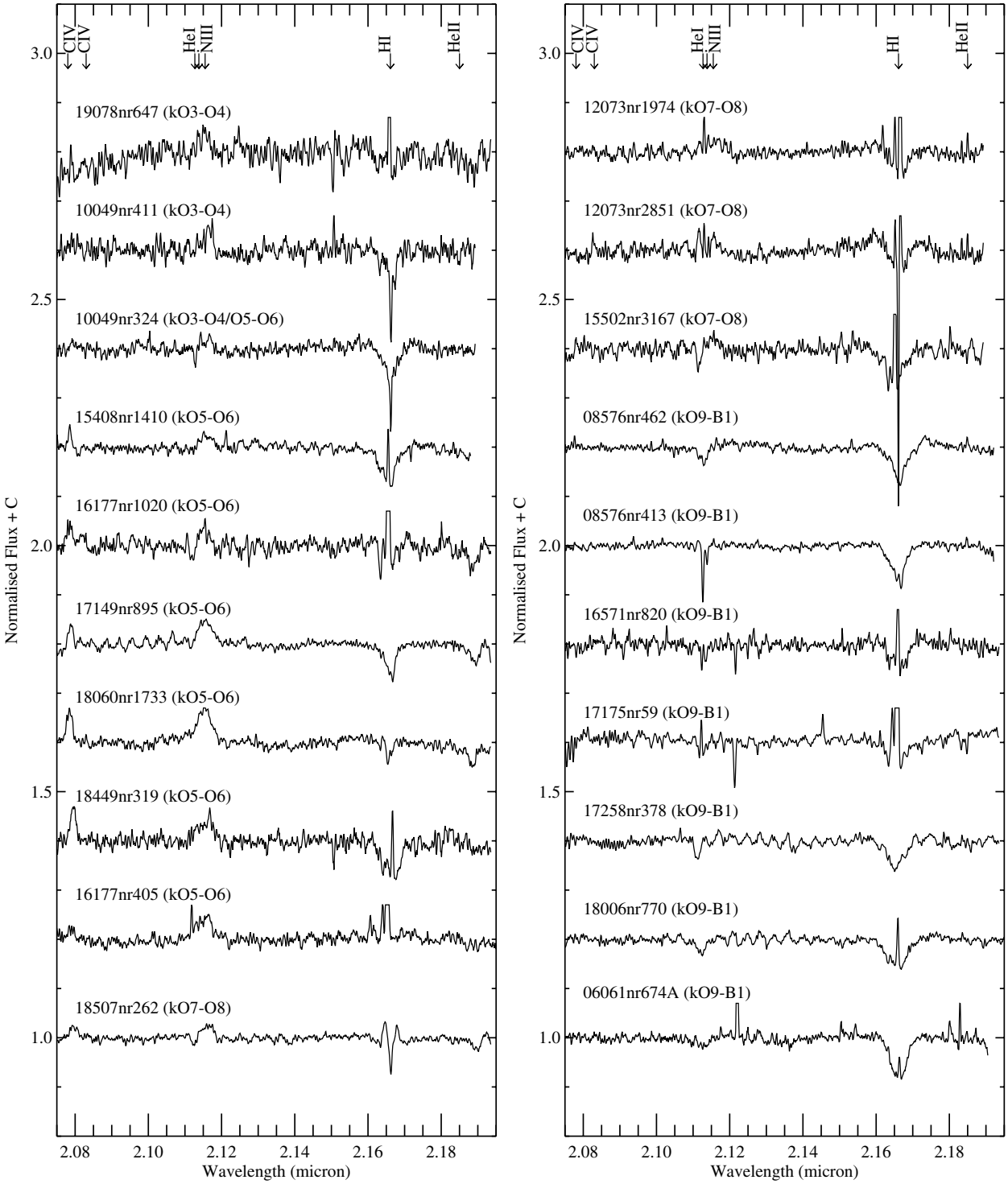

Fig. 4. *K*-band spectra of young OB stars deeply embedded in star-forming regions. The objects are plotted according to their *K*-band spectral type. In the early O stars (*left panel*) C IV and N III are important diagnostics, as well as the He II line. At mid-O spectral type, the He I line becomes an important diagnostic together with the Brγ line (*right panel*). The emission wings present in the Brγ line of 12073nr2851 are likely the result of a bad correction of the Brγ line in the standard star.

(spectro-photometric distance or spectroscopic paralax). By assuming that the stars are all located on the ZAMS, the intrinsic absolute magnitude can be derived. The absolute *K*-band magnitudes for ZAMS stars are taken from Hanson et al. (1997), who follow Massey et al. (1989) for spectral types between O3V and B1V and Kenyon & Hartmann (1995) for the B stars. The $J - K$ colour is almost constant for OB stars ($J - K = -0.2$, Koornneef 1983), allowing a good determination of the extinction towards the OB star.

By comparing the different distance estimates, for more than half of the stars (~60%) the spectro-photometric distance is comparable to the kinematic distance. In a few cases

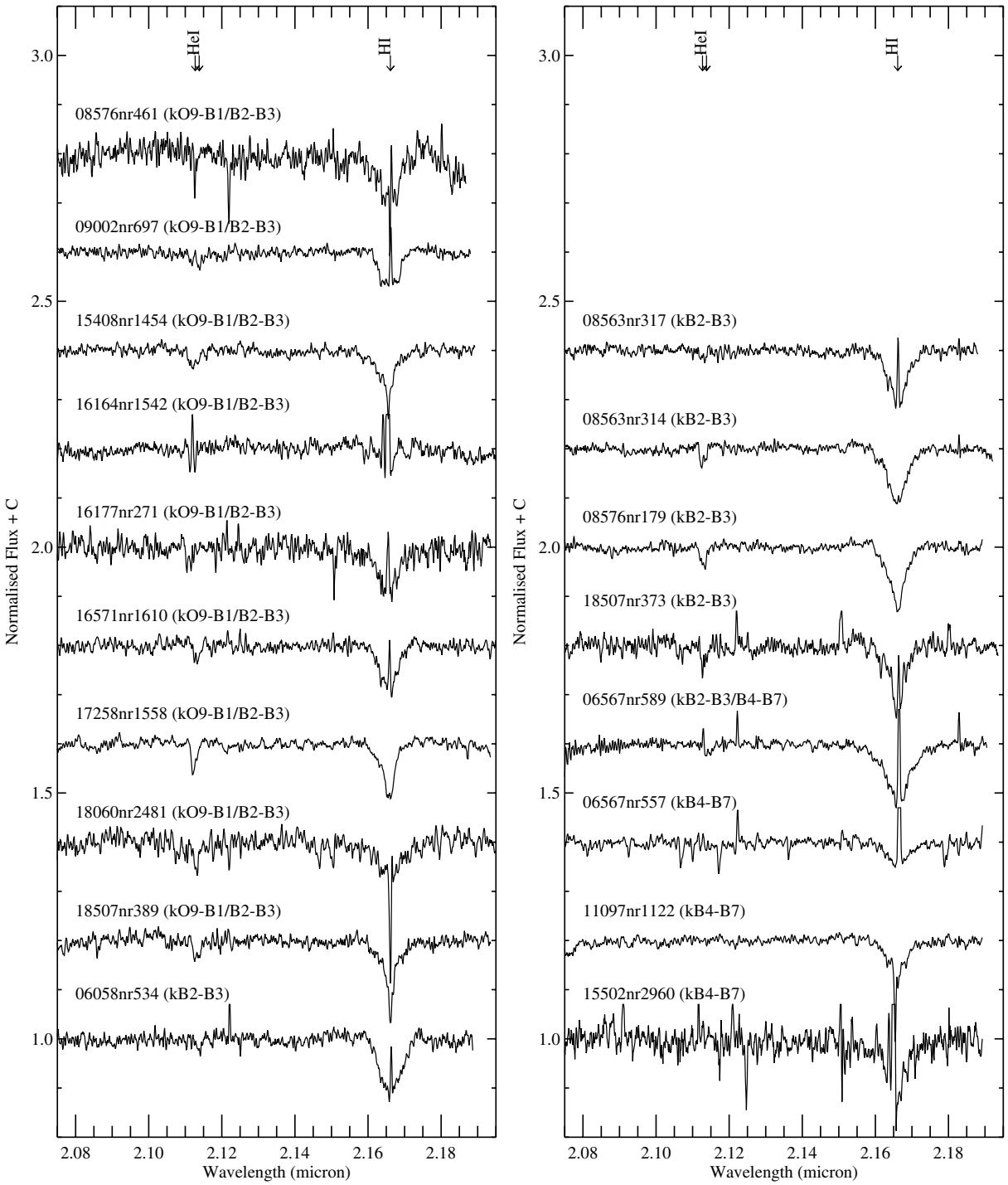

Fig. 5. *K*-band spectra of young OB stars deeply embedded in star-forming regions, continued. In this figure the B stars are plotted. In early-B stars, the He I line is still present (*left panel*), but in the mid-B stars the Brγ line is the only diagnostic line.

(e.g. IRAS 16177-5018 and IRAS 17258-3637) the distance ambiguity can be resolved. For other objects, the literature distance based on optical photometry shows a better match with the spectro-photometric distance (objects in Vela C). Murphy & May (1991) show that IRAS 08563-4711 and IRAS 09002-4732 are both located near the edge of the more distant Vela B cloud (2 kpc). The spectro-photometric distance, however, suggests that IRAS 08563-4711 and IRAS 09002-4732 are located in Vela C (0.7 kpc).

For the other objects, the spectro-photometric distance and the kinematic distance are not consistent with each other. Brand & Blitz (1993) show that the residual radial velocities can be large (upto 40 km s^{-1}) in certain directions, and will introduce a large uncertainty in the determination of the kinematic distance.

Also the distances derived for stars in the same embedded cluster can be different. In four regions, the spectro-photometric distance of one of the stars is not consistent

Table 3. *EW* measurements of the spectral lines detected in the *K*-band spectra of young OB stars. Before measuring the *EW*, the nebular Brγ and He I lines have been subtracted out, if present. The He II line is not covered in the wavelength setting used in visitor mode (indicated with *n* in Col. 6). Emission lines have a negative *EW*. The error on the *EW* takes into account the signal-to-noise ratio and the peak over continuum ratio of the line.

Object	C IV	N III	He I	H I	He II
06058nr534	...	...	0.38 ± 0.15	7.6 ± 0.7	n
06061nr674A	...	...	0.60 ± 0.19	4.1 ± 0.3	n
06567nr557	...	...	...	3.5 ± 0.6	n
06567nr589	...	...	0.43 ± 0.16	10.3 ± 0.6	n
08563nr314	...	...	0.61 ± 0.12	7.0 ± 0.4	n
08563nr317	...	...	0.34 ± 0.14	6.5 ± 0.4	n
08576nr179	...	...	0.71 ± 0.11	6.6 ± 0.3	n
08576nr413	...	...	0.86 ± 0.03	3.7 ± 0.2	n
08576nr461	...	...	0.57 ± 0.11	5.2 ± 1.0	n
08576nr462	...	...	0.68 ± 0.16	3.1 ± 0.3	n
09002nr697	...	...	0.70 ± 0.24	4.9 ± 0.4	n
10049nr324	−0.22 ± 0.12	−0.67 ± 0.16	0.22 ± 0.05	3.0 ± 0.3	n
10049nr411	...	−1.8 ± 0.5	...	2.4 ± 0.6	n
11097nr1122	...	...	...	4.3 ± 0.4	n
12073nr1974		−1.6 ± 0.4	neb	2.5 ± 0.3	n
12073nr2851	...	−1.8 ± 0.2	neb	2.6 ± 0.4	n
15408nr1410	−0.57 ± 0.08	−1.20 ± 0.28	...	3.0 ± 0.3	n
15408nr1454	...	...	1.0 ± 0.22	4.8 ± 0.5	n
15502nr2960	...	...	...	6.1 ± 1.0	n
15502nr3167	...	−0.71 ± 0.35	0.64 ± 0.14	4.9 ± 0.6	n
16164nr1542	...	...	1.1 ± 0.3	4.5 ± 1.5	...
16177nr271	...	...	0.83 ± 0.35	5.4 ± 0.9	...
16177nr405	−0.55 ± 0.22	−2.3 ± 0.4	neb	...	...
16177nr1020	−1.0 ± 0.25	−1.7 ± 0.4	...	2.7 ± 0.5	1.45 ± 0.35
16571nr820	...	...	0.57 ± 0.1	2.4 ± 0.4	...
16571nr1610	...	...	0.66 ± 0.14	5.2 ± 0.4	...
17149nr895	−0.87 ± 0.09	−2.5 ± 0.3	...	2.0 ± 0.2	0.95 ± 0.16
17175nr59	...		0.86 ± 0.14	4.4 ± 0.5	...
17258nr378	...	...	0.73 ± 0.14	3.0 ± 0.4	...
17258nr1558	...	...	0.95 ± 0.10	4.9 ± 0.3	...
17423nr3102	−1.0 ± 0.16	−6.1 ± 0.5	blend	25.4 ± 0.2	0.6 ± 0.16
18006nr770	...	...	0.75 ± 0.36	3.6 ± 0.5	...
18060nr1733	−1.2 ± 0.24	−3.5 ± 0.4	...	0.76 ± 0.2	0.76 ± 0.16
18060nr2481			0.75 ± 0.22	4.9 ± 1.0	...
18449nr319	−1.4 ± 0.2	−2.7 ± 0.7	...	3.9 ± 0.6	...
18449nr335	...	−10.6 ± 0.5	blend	−44.2 ± 1.0	−3.2 ± 0.2
18507nr262	−0.7 ± 0.15	−1.1 ± 0.2	0.12 ± 0.06	??	0.5 ± 0.15
18507nr373	...	...	0.79 ± 0.27	6.6 ± 0.5	...
18507nr389	...	...	0.79 ± 0.26	5.3 ± 0.3	...
19078nr647	...	−1.9 ± 0.6	...	4.0 ± 1.2	1.3 ± 0.5

with the distance derived for the other stars. For example, in IRAS 10049-5657, the spectral type of the two stars (10049nr324 and 10049nr411) is similar, but the *K*-band magnitude differs by 1 mag. The two stars have a similar $J - K$ suggesting that they are confronted with the same amount of extinction, which makes it unlikely that one of the stars is a foreground star (the spectro-photometric distance towards the faintest star, 10049nr411, is similar to the kinematic distance).

Table 4. Classification of the K-band spectra based on EW measurements (Table 3) and classification scheme (Table 1) developed by Hanson et al. (1996). Column 2: the K-band spectral type, Col. 3: the corresponding optical spectral type. Column 4: kinematic distance derived from the radial velocity measurements of Bronfman et al. (1996) and the rotation model of the galaxy of Brand & Blitz (1993). Column 5: adopted distance (Kaper et al. 2005). Column 6: K-band magnitude; Col. 7: $J-K$; Col. 8: the derived visual extinction (A_V). Column 9, the distance based on this spectral classification, assuming that the stars are ZAMS stars (Hanson et al. 1997). † This object is located towards the galactic center.

Object	K-band sp. type	MK sp. type	Kin. dist (kpc)	Dist. (kpc)	K	$J-K$	A_V	Sp. Ph. dist. (kpc)
06058nr534	kB2–B3	B1V–B2.5V	1.0	2.2	10.4 ± 0.02	1.3 ± 0.04	7.3	1.0–1.5
06061nr674A	kO9–B1	O8V–B1V	–	2.2	11.8 ± 0.04	2.0 ± 0.09	11.4	2.3–5.1
06567nr557	kB4–B7	B3V–B7V	2.6	2.3	11.6 ± 0.04	2.6 ± 0.10	14.0	0.8–1.1
06567nr589	kB2–B3/kB4–B7	B1V–B7V	2.6	2.3	10.4 ± 0.02	3.2 ± 0.07	17.3	0.4–0.8
08563nr314	kB2–B3	B1V–B2.5V	2.1	2.0	8.9 ± 0.01	1.4 ± 0.02	7.8	0.5–0.7
08563nr317	kB2–B3	B1V–B2.5V	2.1	2.0	10.0 ± 0.02	2.3 ± 0.04	12.6	0.6–0.9
08576nr179	kB2–B3	B1V–B2.5V	2.2	0.7	9.6 ± 0.01	1.9 ± 0.03	10.5	0.6–0.8
08576nr413	kO9–B1	O8V–B1V	2.2	0.7	7.5 ± 0.01	1.8 ± 0.01	10.4	0.3–0.8
08576nr461	kO9–B1/kB2–B3	O8V–B2.5V	2.2	0.7	12.7 ± 0.06	1.7 ± 0.11	9.8	2.6–8.5
08576nr462	kO9–B1	O8V–B1V	2.2	0.7	7.0 ± 0.01	1.8 ± 0.01	10.4	0.2–0.6
09002nr697	kO9–B1/kB2–B3	O8V–B2.5V	1.9	2.0	10.7 ± 0.03	5.4 ± 0.22	29.0	0.4–1.2
10049nr324	kO3–O4/kO5–O6	O3V–O6.5V	7.1	7.1	10.5 ± 0.02	2.8 ± 0.06	15.7	2.7–4.4
10049nr411	kO3–O4	O3V–O4V	7.1	7.1	11.7 ± 0.04	2.9 ± 0.11	16.2	6.5–7.4
11097nr1122	kB4–B7	B3V–B7V	3.1	2.8	10.5 ± 0.02	2.4 ± 0.05	13.0	0.5–0.7
12073nr1974	kO7–O8	O7V–O8V	11.6	11.6	10.7 ± 0.03	2.3 ± 0.05	13.0	2.8–3.2
12073nr2851	kO7–O8	O7V–O8V	11.6	11.6	10.7 ± 0.03	2.5 ± 0.06	14.1	2.7–3.0
15408nr1410	kO5–O6	O5V–O6.5V	2.6/11.6	2.6	8.6 ± 0.01	2.2 ± 0.02	12.0	1.9–2.4
15408nr1454	kO9–B1/kB2–B3	O8V–B2.5V	2.6/11.6	2.6	9.3 ± 0.01	2.1 ± 0.03	12.5	0.3–1.1
15502nr2960	kB4–B7	B3V–B7V	5.8/8.7	5.8	13.0 ± 0.08	2.6 ± 0.19	14.0	1.5–2.1
15502nr3167	kO7–O8	O7V–O8V	5.8/8.7	5.8	11.8 ± 0.04	1.6 ± 0.19	9.3	5.8–6.6
16164nr1542	kO9–B1/kB2–B3	O8V–B2.5V	3.7/11.4	3.6	11.7 ± 0.04	2.0 ± 0.08	11.4	1.5–4.9
16177nr271	kO9–B1/kB2–B3	O8V–B2.5V	3.4/11.8	3.6	11.8 ± 0.04	3.4 ± 0.14	18.8	1.1–3.4
16177nr405	kO5–O6	O5V–O6.5V	3.4/11.8	3.6	10.8 ± 0.03	≥ 6.7	>35.4	>1.0
16177nr1020	kO5–O6	O5V–O6.5V	3.4/11.8	3.6	11.9 ± 0.04	4.7 ± 0.27	25.5	3.0–3.7
16571nr820	kO9–B1	O8V–B1V	1.9/14.5	1.0	9.3 ± 0.01	2.6 ± 0.03	14.6	0.6–1.4
16571nr1610	kO9–B1/kB2–B3	O8V–B2.5V	1.9/14.5	1.0	11.0 ± 0.03	2.5 ± 0.07	14.1	1.0–3.1
17149nr895	kO5–O6	O5V–O6.5V	2.0/14.6	2.0	8.3 ± 0.01	0.6 ± 0.01	3.9	1.9–2.3
17175nr57	kO9–B1	O8V–B1V	2.0/14.8	2.0	11.5 ± 0.03	6.3 ± 0.5	>33.4	0.6–4.1
17258nr378	kO9–B1	O8V–B1V	2.3/14.6	2.3	10.2 ± 0.02	3.4 ± 0.06	18.8	0.7–1.6
17258nr1558	kO9–B1/kB2–B3	O8V–B2.5V	2.3/14.6	2.3	10.7 ± 0.02	1.9 ± 0.04	10.9	1.0–3.2
17423nr3102	kO5–O6b	O5I–O6I	†	8.5	9.9 ± 0.02	5.3 ± 0.13	28.5	2.6–2.6
18006nr770	kO9–B1	O8V–B1V	1.2	1.9	7.3 ± 0.01	0.9 ± 0.01	5.5	0.4–0.9
18060nr1733	kO5–O6	O5V–O6V	2.1/14.6	2.1	9.0 ± 0.01	2.9 ± 0.03	16.2	1.4–1.6
18060nr2481	kO9–B1/kB2-B3	O8V–B2.5V	2.1/14.6	2.1	11.1 ± 0.03	3.5 ± 0.11	19.3	0.7–2.4
18449nr319	kO5–O6	O5V–O6V	5.9/8.7	4.3	10.8 ± 0.03	2.4 ± 0.06	13.5	3.8–4.3
18449nr335	WN7	WN7	5.9/8.7	4.3	8.5 ± 0.01	7.0 ± 0.17	–	
18507nr262	kO5–O6	O5V–O8V	3.7/10.3	3.7	9.4 ± 0.01	4.3 ± 0.07	23.4	0.9–1.3
18507nr373	kB2–B3	B1V–B2.5V	3.7/10.3	3.7	12.3 ± 0.05	5.4 ± 0.49	28.6	0.8–1.1
18507nr389	kO9–B1/kB2–B3	O8V–B2.5V	3.7/10.3	3.7	11.3 ± 0.03	3.8 ± 0.14	20.9	0.7–2.4
19078nr647	kO3–O4	O3V–O4V	0.1/12.3	11.4	13.2 ± 0.07	4.4 ± 0.5	23.9	8.4–9.6

The magnitude difference could be explained if 10049nr324 is an equal-mass binary (2 O3-O4 stars) which would result in an increase by 0.7 mag.

Also in IRAS 08576-4334 we derive for one of the stars a different spectro-photometric distance. In this cluster we took spectra of 4 late-O, early B stars. Three stars have a spectro-photometric distance consistent with the distance to the Vela Molecular Ridge. Like in IRAS 10049-5657, all the objects are suffering from the same amount of extinction (Col. 8, Table 4). The magnitude of 08576nr461 is 3−4 mag too faint. Although

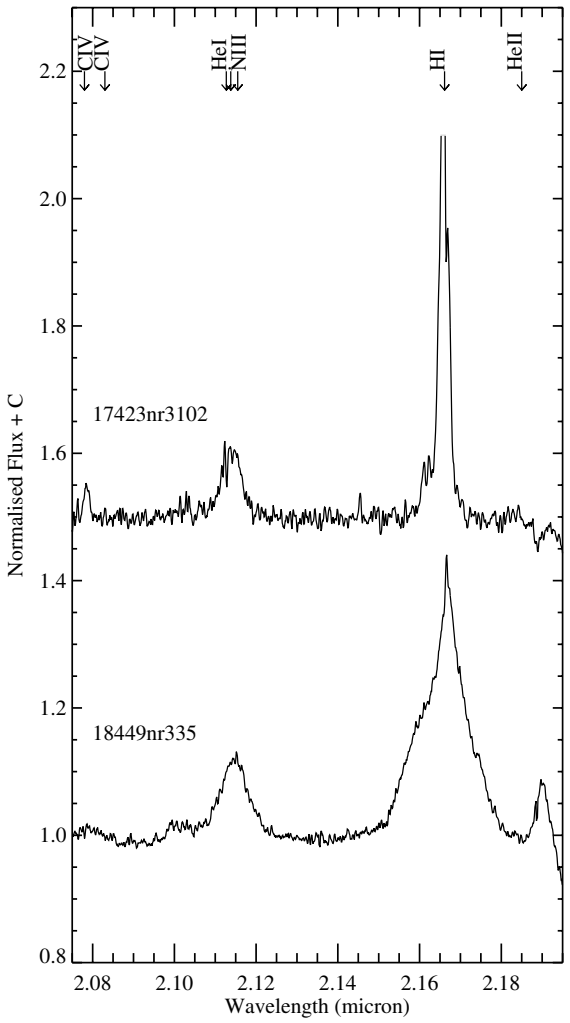

Fig. 6. *K*-band spectra of two early-type stars showing emission lines. The spectrum of 17423nr3102 shows the photospheric features of a kO5-O6b star, the Brγ emission line likely indicates a strong stellar wind. The bottom spectrum (18449nr335) has the characteristics of a WN star. Blum et al. (1999) classify the spectrum as WN7.

the spectrum has a low S/N, the He I line is detected, which determines the spectral type to be kO9-B1/kB2-B3. Even if the He I line were not present and the star would be classified as kB4-B7, the distance does not match. It likely is a background star; in this direction, one looks along a spiral arm resulting in the projection of several star-forming regions. Also for 15408nr1454 and 15502nr2960 the derived distances are not consistent with the distances for the other stars in the same cluster.

4. *K*-band spectra of near-infrared counterparts of UCHII regions

The comparison done in Kaper et al. (2005) between the near-infrared images and the UCHII radio observations (Wood & Churchwell 1989b; Kurtz et al. 1994; Walsh et al. 1998, and Kurtz, priv. comm.) shows that 21 UCHII radio sources have a near-infrared counterpart. For 7 of these regions the near-infrared counterpart is a compact cluster of stars, and the radio emission is extended. The linear size derived for some of these objects suggests that they are not in the UCHII stage anymore. For instance, by adopting the distance determination of 7.3 kpc to IRAS 06412-0105, the extent of the radio emission is ~1 pc. For IRAS 12073-6233, which is at 11.6 kpc, a size of 6×4 pc is found (i.e. much larger than 0.1 pc).

Towards the other UCHII radio sources, no cluster is detected, but the near-infrared counterparts are point sources. For 7 of these objects we have taken *K*-band spectra which are shown in Fig. 7. All but one spectra are dominated by nebular emission. Strong, narrow, Brγ and He I emission are seen in the spectra. A more careful inspection of these seven spectra reveals that in one case (17175nr59) weak Brγ photospheric absorption is present. This star is classified as a kO9-B1. Another object (06061nr676) displays a broad and spectrally resolved Brγ line, and has the characteristics of a massive Young Stellar Object; this object is discussed in detail in Bik et al. (2005). For comparison we include these objects in Fig. 7.

Comparison of the magnitudes and colours of the three types of objects (OB stars, nebular spectra and massive YSO candidates) found in our spectroscopy survey shows that the near-infrared counterparts of UCHII regions have on average the faintest *K* magnitude and the reddest $J-K$ colour. This suggests that these sources suffer from more extinction than the OB stars and massive YSOs do. The near-infrared continuum of the counterparts of the UCHII regions is likely not dominated by the stellar continuum as no photospheric features are detected. The slope of the continuum is likely much redder than that of the OB stars; the continuum will be caused by free-free emission of the UCHII region in combination with hot dust heated by the ionising star in the UCHII region or scattered light.

Since the UCHII regions are often found in areas with extended radio and associated near-infrared line emission from a larger, (evolved) H II region, the question arises what the origin is of the nebular emission lines detected towards the UCHII regions. Inspection of the spatial distribution of the nebular emission of our 7 sources indicates that in almost all cases the line emission is peaked at the position of the radio source. The He I emission, if present, also peaks at the radio source.

In addition, in one case we can compare the width of the radio recombination lines with that seen in our spectra. For W49A South our spectrum indicates a width of 90 km s^{-1}, in agreement with the width seen at radio frequencies (de Pree et al. 1997). We conclude that there is good reason to assume that at least in some UCHII regions the near-infrared emission lines are caused by the same gas producing the radio emission.

Therefore, the nebular lines originating from the UCHII region can be used to estimate the spectral type of the underlying ionising source. The presence of He I is indicative of stars with a spectral type earlier than O9V (Hanson et al. 2002). This is confirmed by the weak He I line present in the spectrum of the O9-B1V star (17175nr59). This means that, according to their strong He I emission, most of the stars embedded inside the UCHII regions are of early O spectral type. This preference to detect the hottest O stars is not surprising, since these objects will produce the brightest UCHII regions and will also produce strong nebular line emission in the near-infrared. In

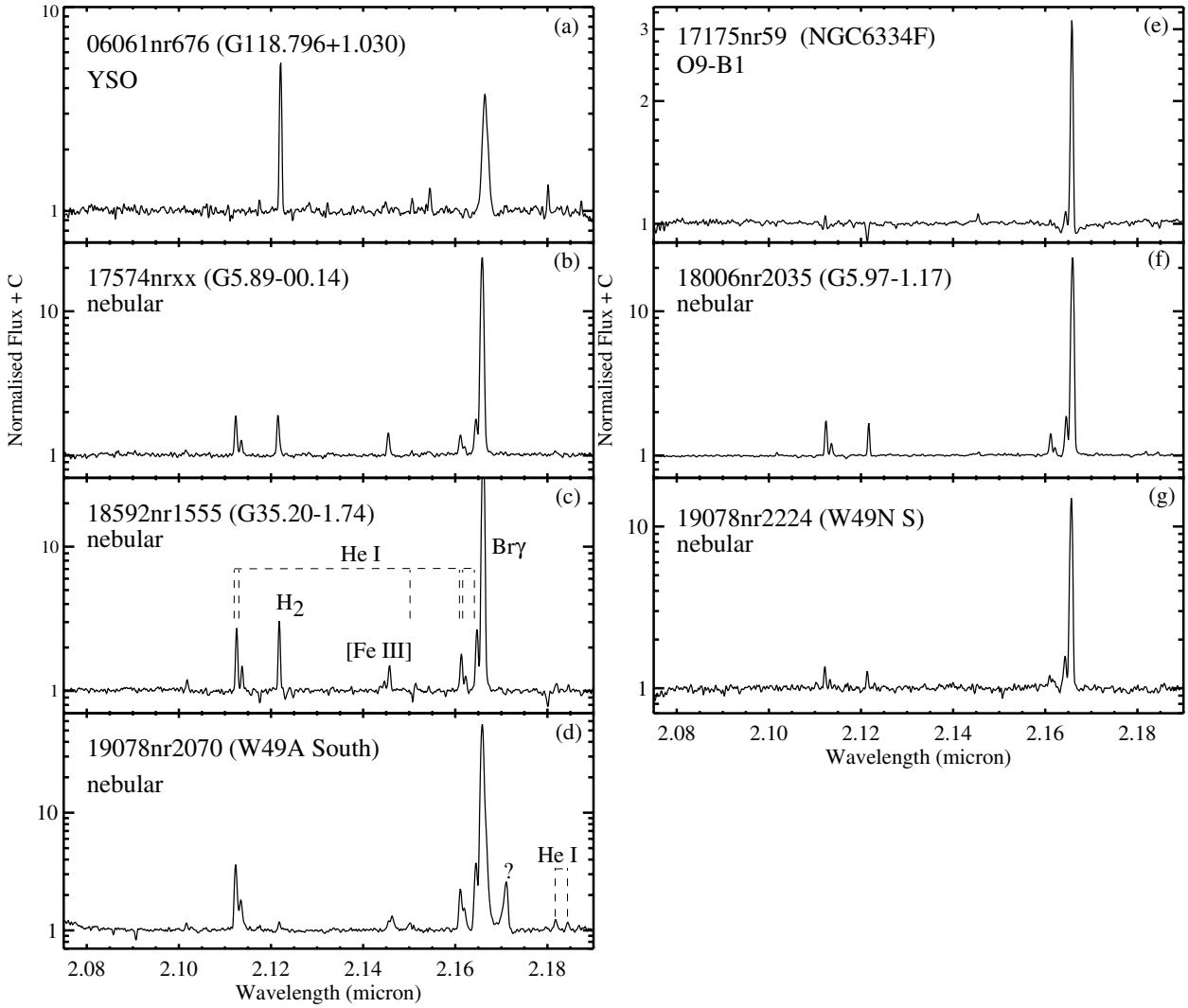

Fig. 7. *K*-band spectra of the near-infrared counterpart of ultra-compact radio source. In the upper-left corner of each panel the name of the source is given with the name of the UCHII radio source in parentheses. The flux scale is logarithmic. The line identifications are given in panels **c)** and **e)**. The line at 2.171 μm in panel **e)** could not be identified.

contrast, late O or B stars will in general not be easily detected as UCHII regions. Their immediate environment, however, will contain remnants of the star formation process for a much longer period of time than that of the hottest O stars. Indeed, the YSO candidates are often found to be of B spectral type and are generally not UCHII regions.

5. Ionising properties of the embedded clusters

One of the results of the near-infrared imaging survey of Kaper et al. (2005) is that the UCHII regions are not isolated, but are located inside more extended regions of (massive) star formation. In almost all these regions embedded clusters are detected. The properties of these clusters are discussed in detail in Kaper et al. (2005). The majority of the spectra presented in this paper do not correspond to the near-infrared counterpart of the UCHII region detected in the radio, but to massive stars located inside the cluster associated with the UCHII region.

For the determination of the ionising power of these clusters, the UCHII radio observations are not suitable. Only small spatial scales are resolved by these interferometric radio surveys. The radio flux of the more extended H II region is not picked up (see e.g. Kurtz et al. 1999). Therefore, we use the radio measurements presented by Caswell & Haynes (1987). These are single dish observations with a typical spatial resolution of 1′, which makes the observations more compatible with the IRAS observations. The near-infrared images presented in Kaper et al. (2005) cover an area of $5 \times 5'$, an area comparable on the sky to the radio and infrared measurements.

In Cols. 2 and 3 of Table 5 the spectral types are given based on the radio and infrared luminosity. The determination of the radio and infrared spectral type depends on several assumptions which do not have to be valid. E.g., one assumes that only one star is responsible for the radio and infrared flux. The radio and infrared spectral types have to be considered as upper limits in this case. In the regions where the spectral type is estimated to be earlier than O3V (e.g. IRAS 10049-5657), obviously a

Table 5. Spectral type derived using radio and infrared diagnostics and compared with the OB stars found in the region by means of *K*-band spectroscopy. Column 1: object; Col. 2: radio spectral type of the extended H II region based on Caswell & Haynes (1987); Col. 3: infrared spectral type based on the IRAS flux. The IRAS luminosity is calculated using the formula of Sect. 7.6 in Cox (2000). The spectral types are derived using the stellar parameters of Smith et al. (2002) for the O3 – B1.5 stars and Aller et al. (1982) for the B stars; Col. 4: the earliest *K*-band spectral type of the OB star located in this region. † A giant H II region is defined by the fact that it emits more than 10^{50} Lyman continuum photons s^{-1} (e.g. Blum et al. 1999).

IRAS name	Radio Sp Type	IRAS Sp Type	*K*-band Sp. Type	Ionising source
06058+2138		B1.5V/B2V	B1V-B2.5V	06058nr534 is the main ionising source. Massive YSOs 06058nr221 and 06058nr227 have mid – late B spectral type.
06061+2151		B2V	O8V-B1V	06061nr674A is the main ionising source. Spectral type is not consistent with class I nature (Anandarao et al. 2004).
06567-0355	B1V(W86)	B1.5-B2	B1V-B7V	Cluster has ultra compact radio counterpart.
08563-4711	O8V	B1V	B1V-B2.5	two stars are ionising this region, spectral type estimates of Liseau et al. (1992) (B5V and A5V) are not consistent.
08576-4334	O9V	B2V	O8V-B1V	08576nr413 and 08576nr462 (O8V-B1V) are located in the center, massive YSOs 08576nr292 and 08576nr408 in the outskirts of the cluster. The stars in the center are likely the main ionising sources.
09002-4732	O8.5V	O8.5V	O8V-B2.5V	Apai (2004) conclude that this region is dominated by one ionising source coinciding with the UCHII region. 09002nr697 is located in the outskirts of the nebula.
10049-5657	<O3V	<O3V	O3V-O4V	Giant H II region†. In the CMD of this field (Kaper et al. 2005) a reddened main sequence is clearly visible. The spectral type determination of two O3V-O4V stars (10049nr411 and 10049nr324) shows that this cluster must be very massive.
11097-6102	<O3V	O4V	B3V-B7V	Giant H II region† (NGC 3576), ionising sources are still heavily embedded and not visible in the near-infrared (Figuerêdo et al. 2002).
12073-6233	<O3V	<O3V	O7V-O8V	Giant H II region†. 12073nr1974 and 12073nr2851 are located in center of cluster.
15408-5356	O4.5V	O7.5V	O5V-O6.5V	15408nr1410 likely the ionising source, in center of cluster.
15502-5302	O4V	<O3V	O7V-O8V	15502nr3167 not the ionising source, the stars in center of cluster show nebular spectra, apparently too embedded to be observed in the near-infrared.
16164-5046	O4V	O4V	O8V-B2.5V	16164nr1542 is not the ionising source. 16164nr3636(YSO) might be of mid-O spectral type.
16177-5018	O3V	O4V	O5V-O6.5V	16177nr1020 and 16177nr271 ionising sources.
16571-4029	O9V	B1V	O8V-B1V	16571nr820 and 16571nr1610 ionising sources.
17149-3916	O8V	B0V	O5V-O6.5V	*K*-band spectral type not consistent with other determinations.
17175-3544	<O3V	O8V	O8V-B1V	*K*-band spectral type consistent with infrared spectral type.
17258-3637	O6V	O7.5V	O8V-B1V	Main ionising source still embedded, UCHII region has no near-infrared counterpart.
17423-2855				Located in Galactic Center (Cotera et al. 1999).
18006-2422		O9.5V	O8V-B1V	18006nr770 is Her 36, ionising source of M8.
18060-2005		O9.5V	O5V-O6V	*K*-band spectral type not consistent with infrared spectral determination.
18449-0158		B0.5V	O5V-O6V	W43, giant H II region† (Blum et al. 1999). 18449nr319 is one of the ionising sources.
18507+0110		O3V	O5V-O6V	Not related to UCHII region. Western part of nebula likely ionised by 18507nr262
19078+0901	<O3V	<O3V	O3V-O4V	W49A is one of the most luminous giant H II regions† in our galaxy (Conti & Blum 2002). 19078nr647 is object 1 in Conti & Blum (2002) and one of the ionising sources.

cluster is required to ionise the H II region and heat the surrounding dust. Based on the amount of Lyman continuum photons ($>10^{50}$ photons s^{-1}) some of these regions are classified as giant H II regions (e.g. Blum et al. 1999).

Another assumption used to determine the (radio) spectral type is that the H II region is ionisation bounded (no FUV photons are leaking) and dust-free (no FUV photons are absorbed by dust). For the determination of the infrared spectral type the

assumption is that all the radiation from the star is reprocessed and emitted at infrared wavelengths. If these assumptions are not valid, the radio and infrared spectral types have to be seen as lower limits (i.e. the ionising star is of earlier spectral type).

In Col. 4 of Table 5 the spectral type of the hottest OB star found by our spectroscopic survey is given. It turns out that in about 50% of the H II regions we have identified the main ionising source(s). This finding would suggest that the IRAS fluxes of about 50% of the sources is dominated by the dust heated by the cluster members instead of the emission of an UCHII region. In some regions, however, the ionising sources are likely heavily embedded and not visible in the near-infrared (e.g. IRAS 11097-6102).

6. Discussion

We have obtained K-band spectra of deeply embedded massive stars in IRAS sources with UCHII colours. The stars are classified using the classification scheme developed by Hanson et al. (1996). The question is whether the properties of the young OB stars resemble those of the more evolved OB stars in OB associations and the field population. Also, do they drive a normal stellar wind at such a young age? We will discuss the spectral properties of the stars as well as age estimates of the clusters and the implications for the UCHII lifetime problem.

6.1. Stellar wind properties

The OB stars in this study are classified following Hanson et al. (1996). In general these stars have K-band spectra similar to field stars. To determine whether the properties of the young, embedded OB stars are different from those in the field, the K-band spectra of our sources are compared with K-band spectra of field stars, like the spectra in Hanson et al. (1996). These are, however, also used to classify the spectra. This means that the lines used for the classification cannot be used for this comparison. For example, in the spectral classes kO9-B1 and later, the strength of Brγ is used for spectral classification and a different behaviour of Brγ (i.e. due to a stronger stellar wind) would result in an erroneous classification. For the early types (kO3-O4 to kO7-O8), however, more lines are present and Brγ does not need to be used for the spectral classification, so the properties of this line can be compared with those of the field stars.

A few stars, classified as early O stars, show a peculiar behaviour of the Brγ line (Sect. 3.2): the line is not present, or in emission. Also the He II line in one of the objects (16177nr405) is either not present, or very weak. One of the possible explanations for this effect is that the stars have a strong stellar wind and that the photospheric Brγ absorption is filled in by stellar wind emission. This would only happen, however, if the wind mass loss rate is as high as that of OB supergiants (cf. Puls et al. 1996; Lenorzer et al. 2004). The He II line is not formed in the wind, but originates in the stellar photosphere. This line should be much less affected by the stellar wind than Brγ. Only a very high wind density makes the He II line turn into emission. A similar effect is found in the optical spectrum, where the He II line at 4686 Å turns into emission with increasing stellar wind. Veiling by dust or free-free emission of the surrounding H II region seems unlikely as the intrinsically weak lines like C IV and N III are detected.

Contrary to the suggestion found in our data that the young stars possess a relatively strong wind, evidence has been presented that in the SMC a class of young OB stars (Vz stars) is found that have unusually weak winds for their spectral type (Heydari-Malayeri et al. 2002; Martins et al. 2004). The suggestion is that these stars are located very close to or even on the ZAMS. The authors also suggest that these objects might be sub-luminous.

To disthinguish between these two scenarios for the stellar wind of the youngest OB stars, a careful analysis of spectral lines sensitive to the wind density is needed. For these deeply embedded stars, the UV spectrum or the Hα line which are usually employed to determine the stellar wind properties are not available. The Brγ line in the K-band is not the best line for this analysis. Brα in the L-band is more sensitive to the stellar wind density (Lenorzer et al. 2004).

6.2. Binarity and stellar rotation

The primordial binary fraction and the rotation rate of newly formed massive stars carry important information regarding the star formation process. Naively one would expect that newborn stars rotate more rapidly than evolved stars. Furthermore, the fact that the majority of massive stars are members of a binary/multiple system indicates that many young massive stars should belong to binary systems as well.

The binarity of the OB stars detected in massive starforming regions provides a strong constraint on formation scenarios of massive stars (e.g. Zinnecker 2003). Observations of e.g. the massive stars in the Orion Nebula Cluster show that all stars belong to double or multiple systems (Preibisch et al. 1999). Studies to determine the fraction of spectroscopic binaries among bright O stars show that at least 35% of the field O stars have a companion, while the fraction of spectroscopic binaries in the case of young stellar clusters can get as high as 60% (Mason et al. 1998). The contribution from single-line spectroscopic binaries (SB1s) and double-line specroscopic binaries (SB2s) is roughly equal.

The OB stars presented in this paper all belong to young stellar clusters, suggesting that also among these massive stars a large fraction is member of a binary system. With spectra taken at only one epoch, we will not be able to detect the SB1s. To this aim we carried out second-epoch observations of most of the OB stars in our sample (Apai et al., in prep.). For two out of 16 targets a shift in radial velocity has been measured, making the targets SB1 candidates. We find no evidence for double-lined spectroscopic binaries in our sample. Obviously, our spectra have limited spectral resolution and signal to noise, and include only a few photospheric lines. Also, the detectability of an SB2 depends on the ratio in luminosity between the two components and the eccentricity of the system.

To illustrate the variation in projected rotational velocity in our sample, the He I lines at 2.1127 and 2.1138 μm are plotted on a velocity scale for four different objects. In the top

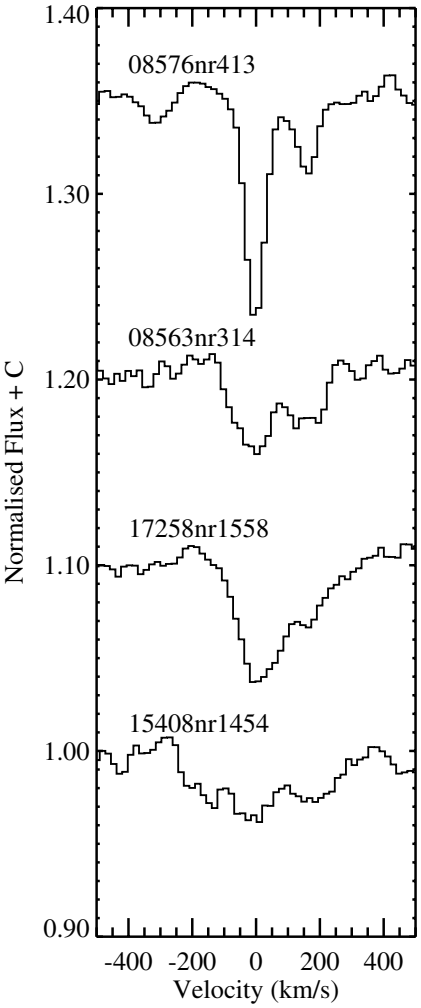

Fig. 8. Profiles of the He I lines at 2.1128 and 2.1138 μm. The different width of the lines reflects their rotation properties.

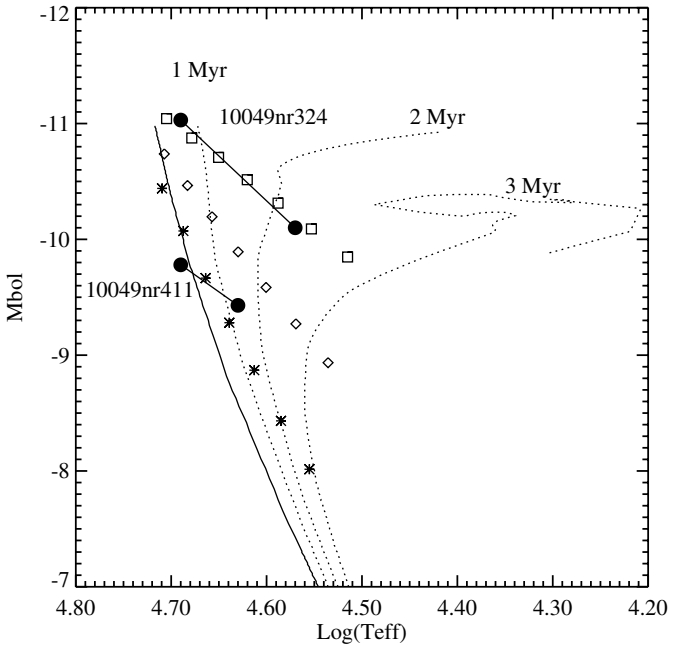

Fig. 9. Upper part of the HR-diagram. The full line represents the ZAMS, the other lines are the isochrones of 1, 2 and 3 million years. The data are taken from Lejeune & Schaerer (2001). The location of the two objects in IRAS 10049-5657 is represented by two bullets connected with a line. The end points of the lines correspond to the location of the earliest and latest spectral type consistent with the observed spectrum. The temperatures are taken from Martins et al. (2002), and the values for $V - K$ and the bolometric correction from Koornneef (1983) and Aller et al. (1982), respectively. Overplotted are the models for O stars taken from Lenorzer et al. (2004). The crosses correspond to the position of the luminosity class V models for different $T_{\rm eff}$ and luminosity, while the diamonds and squares represent the locations of the giant and supergiant models, respectively.

spectrum the two He I lines are clearly separated, while in the bottom spectrum the two He I lines are severely blended due to the rotational broadening. Proper measures of the value of $v \sin i$ in these stars should be obtained using more lines and higher spectral resolution, but at first inspection the projected rotational velocities do not seem to be different from those measured from main-sequence O-type stars (Penny 1996).

6.3. Cluster age

Despite the fact that most of the OB stars in our sample are not directly associated with an UCHII region, their location deeply embedded inside star forming regions (see Sect. 5) still suggests that these objects are young. Studies of the embedded population in W31 (Blum et al. 2001) and M17 (Hanson et al. 1997) show that these regions are young and have an age of ∼1 million year. These age determinations were based on the location of the stars in the HRD with respect to isochrones. However, isochrone fitting is not reliable anymore for very young clusters (≤1−2 Myr) when only massive stars are used. The isochrones are located too close to each other in the HR-diagram and the physical parameters for the hottest stars are not well known. Comparing the position of low-mass stars with the pre-main sequence tracks will improve the age determination, as well as allow for a measurement of the disk fraction in the young clusters (e.g. Lada & Lada 2003).

The method of isochrone fitting is illustrated in Fig. 9. Two objects, 10049nr324 (O3-O6.5V) and 10049nr411(O3-O4V), are plotted in the HR-diagram together with isochrones (Lejeune & Schaerer 2001). The solid line is the ZAMS, the other isochrones are those of 1, 2 and 3 million year. The two massive stars located in IRAS 10049-5356 (plotted with a "•" in Fig. 9) are located close to the upper end of the ZAMS. Their location in the HR-diagram is consistent with an age younger than ∼2 million years. We note that the location of 10049nr324 in the HR-diagram implies a luminosity of about $3{-}4 \times 10^6\ L_\odot$. This would make this object one of the most luminous stars known in the galaxy comparable to the enigmatic object η Car ($\log(L/L_\odot) \sim 6.5{-}6.7$). Remarkably, the Br$\gamma$ line of 10049nr324 shows one of the strongest absorption profiles observed in any object classified as O3 (Hanson et al. 1996). However, at such extreme luminosity it is unlikely that the radiation driven wind would be too weak to produce Brγ emission. This is confirmed by model calculations of Lenorzer et al. (2004), who predict that Brγ should be in

emission for supergiants. For any combination of L and $T_{\rm eff}$ consistent with the observations of 10049nr324, Brγ should be in emission, or at least only weakly in absorption, contrary to what is observed.

There are two possible solutions to this problem. The distance estimate of the cluster may be in error. However, a distance of ∼3 kpc would be required to be consistent with a position of 10049nr324 on the ZAMS, which would move 10049nr411 significantly below the ZAMS. Alternatively, 10049nr324 could be a spectroscopic binary consisting of 2 equal mass O3-O4 stars. Both solutions place one or both stars very close to the ZAMS, suggesting an age of ∼1 Myr or less.

6.4. UCHII lifetime problem

A fundamental problem with UCHII regions is related to their lifetime. If the young and ultra-compact H II region expands due to over-pressure with roughly the sound speed, the lifetime of an UCHII is expected to be on the order of 10^4 years. Using the IRAS colour−colour criterium of Wood & Churchwell (1989a), the number of UCHII regions in the galactic disk relative to the number of emerged O stars implies a duration of the embedded phase on the order of several 10^5 year, although a more refined evaluation shows that this might be one order of magnitude less (Comerón & Torra 1996).

Several confining mechanisms have been proposed to extend the UCHII lifetime: wind bow shocks generated by the supersonic motion of the stars ($v_{\rm sound} \simeq 0.2$ km s^{-1}, van Buren et al. 1990), evaporation of dense clumps or a circumstellar disk which mass-loads the stellar wind (Hollenbach et al. 1994), or an initial evolution taking place in a very dense molecular cloud core.

Kaper et al. (2005) show that in 75% of the observed fields a cluster is identified towards the location of the IRAS source. In Sect. 5 it is shown that in 50% of these clusters we have detected the main ionizing source. In these cases the infrared luminosity as measured by IRAS could be explained by the spectroscopically identified OB stars in the clusters. This would mean that in these cases the IRAS flux is not related to an UCHII radio source but is caused by the OB stars located in the embedded cluster heating the surrounding dust.

Estimates of the lifetime of these embedded clusters are of the order of 10^6 years (Hanson et al. 1997; Blum et al. 2001). As this lifetime is much larger than those of the UCHII regions this would help to resolve the "UCHII lifetime problem". High spatial resolution observations in the mid-infrared with e.g. Spitzer are required to test this hypothesis.

6.5. Ionising properties of the UCHII regions

It is interesting to compare the different diagnostics concerning the stellar content of the fields we studied, in relation to the spatial scales they refer to.

The IRAS sources refer to scales of ∼1′, comparable to those of the embedded clusters. Similar scales apply to the single dish radio measurements (Caswell & Haynes 1987). As noted in Sect. 5, the spectral types derived from both diagnostics are in reasonable agreement, suggesting that on this scale we pick up optically thin emission which is reprocessed light from the less embedded OB stars.

On small scales, we find radio emission from UCHII regions whose radio continuum slope suggests that high-density, ionised gas is present. We often find hot O stars as the ionising sources of the UCHII regions. However, due to the optically thick nature of the radio continuum, the contribution of these sources to the total radio luminosity of the cluster is modest. Energy balance, however, requires that the luminosity of these embedded O stars is re-emitted at long wavelengths, i.e. far-infrared or mm. Since the IRAS flux can roughly be accounted for by the reprocessed light from the less embedded population, it may be that the reprocessed light of the more embedded sources is emitted at wavelengths longwards of 100 μm, outside the IRAS wavelength range. This can be tested using e.g. HERSCHEL or ALMA observations.

7. Conclusions

In this paper, we present the K-band spectra of young OB stars deeply embedded inside IRAS sources with UCHII colours. K-band spectra of the actual near-infrared counterparts of the UCHII radio sources are also presented and discussed. The results can be summarised as follows:

- 38 OB type stars are identified inside massive star forming regions. They are classified based on the classification scheme of Hanson et al. (1996).
- The K-band spectra of the OB stars are in general similar to those of the (more evolved) OB stars located in OB associations and the field. The K-band spectral properties of the very young OB stars are already indistinguishable from those of the more evolved stars.
- The spectra of a few O5-O6 stars suggest that these stars posses stronger winds than usually encountered in these stars. This finding needs to be confirmed by further observations of e.g. the Brα line.
- Distances to the OB stars are derived using the "spectroscopic parallax" method. In 60% of the regions this distance is consistent with the kinematic distance or other determinations encountered in the literature. The distance determination towards the objects in the Vela Molecular Ridge suggest that IRAS 08563-4711 and 09002-4732 are located in the Vela C cloud instead of the more distant Vela B cloud.
- Comparison of the position of some of the OB stars with theoretical isochrones show that these regions are likely very young, less than 1−2 million years. This method to derive ages suffers from substantial uncertainties due to the contribution from binaries and from fore- or background sources.
- The differences in the line profiles of the He I 2.112 and 2.113 lines reflect the difference in rotational broadening of the stars. At first sight, the projected rotational velocities of the young OB stars do not differ from those measured from main-sequence OB stars.

- In most of the clusters (50%), the ionising source is identified by means of our K-band spectroscopy. The K-band spectral type of the OB star(s) is in most cases similar to the spectral type derived from the infrared luminosity and the single-dish radio observations. This implies, in these cases, that the infared flux is produced by the embedded cluster and not by an associated UCHII region. This could help to resolve the UCHII lifetime problem as the embedded clusters have a lifetime of 10^6 years compared to 10^4 years of the UCHII regions.
- The K-band spectra of 7 point sources which are the near-infrared counterparts of UCHII radio sources show that the majority of these regions are dominated by nebular spectra. The He I lines present in 6 of these objects suggest that O stars are located inside these regions.
- Despite the fact that these UCHII regions include O stars, these stars are not dominating the single-dish radio flux as their H II regions are still partially optically thick. The single-dish radio observations are dominated by the optically thin gas ionised by the OB stars in the cluster containing the UCHII region.
- The infrared flux is also dominated by the dust heated by the stars in the cluster instead of the UCHII region. This suggests that the UCHII regions emit most of their flux at far-infrared and sub-mm wavelengths.

Acknowledgements. AB acknowledges financial support from the DFG during a two-month visit at ESO Headquaters. L.K. has been supported by a fellowship of the Royal Academy of Arts and Sciences in The Netherlands. The authors thank the VLT staff for support and help with the observations. Rens Waters, Alex de Koter, Annique Lenorzer and Fernando Comerón are thanked for stimulating discussions. We thank Elena Puga Antolin for help with the identification of the near-infrared counterparts of the UCHII regions. We thank the anonymous referee for his/her suggestions to improve the paper. NSO/Kitt Peak FTS data used here were produced by NSF/NOAO. MMH acknowledges support from the National Science Foundation, Grant No. 0094050.

References

Aller, L. H., Appenzeller, I., & Baschek, B. e. a., eds. 1982, Landolt-Bornstein: Numerical Data and Functional Relationships in Science and Technology
Anandarao, B. G., Chakraborty, A., Ojha, D. K., & Testi, L. 2004, A&A, 421, 1045
Apai, D. 2004, Ph.D. Thesis
Beltrán, M. T., Cesaroni, R., Neri, R., et al. 2004, ApJ, 601, L187
Bik, A., & Thi, W. F. 2004, A&A, 427, L13
Bik, A., Lenorzer, A., Kaper, L., et al. 2003, A&A, 404, 249
Bik, A., Kaper, L., & Waters, L. B. F. M. 2005, A&A, submitted
Blum, R. D., Damineli, A., & Conti, P. S. 1999, AJ, 117, 1392
Blum, R. D., Damineli, A., & Conti, P. S. 2001, AJ, 121, 3149
Brand, J., & Blitz, L. 1993, A&A, 275, 67
Bronfman, L., Nyman, L.-A., & May, J. 1996, A&AS, 115, 81
Caswell, J. L., & Haynes, R. F. 1987, A&A, 171, 261
Chini, R., Hoffmeister, V., Kimeswenger, S., et al. 2004, Nature, 429, 155
Churchwell, E. 2002, ARA&A, 40, 27
Clark, J. S., & Steele, I. A. 2000, A&AS, 141, 65
Comerón, F., & Torra, J. 1996, A&A, 314, 776
Conti, P. S., & Blum, R. D. 2002, ApJ, 564, 827
Cotera, A. S., Simpson, J. P., Erickson, E. F., et al. 1999, ApJ, 510, 747
Cox, A. N. 2000, Allen's astrophysical quantities (Allen's astrophysical quantities, 4th edition, ed. A. N. Cox (New York: AIP Press, Springer)
de Pree, C. G., Mehringer, D. M., & Goss, W. M. 1997, ApJ, 482, 307
Figuerêdo, E., Blum, R. D., Damineli, A., & Conti, P. S. 2002, AJ, 124, 2739
Hanson, M. M., Conti, P. S., & Rieke, M. J. 1996, ApJS, 107, 281
Hanson, M. M., Howarth, I. D., & Conti, P. S. 1997, ApJ, 489, 698
Hanson, M. M., Luhman, K. L., & Rieke, G. H. 2002, ApJS, 138, 35
Heydari-Malayeri, M., Rosa, M. R., Schaerer, D., Martins, F., & Charmandaris, V. 2002, A&A, 381, 951
Hollenbach, D., Johnstone, D., Lizano, S., & Shu, F. 1994, ApJ, 428, 654
Kaper, L., Bik, A., Comerón, F., & Hanson, M. M. 2005, A&A, submitted
Kenyon, S. J., & Hartmann, L. 1995, ApJS, 101, 117
Koornneef, J. 1983, A&A, 128, 84
Kurtz, S., Churchwell, E., & Wood, D. O. S. 1994, ApJS, 91, 659
Kurtz, S. E., Watson, A. M., Hofner, P., & Otte, B. 1999, ApJ, 514, 232
Lada, C. J., & Lada, E. A. 2003, ARA&A, 41, 57
Lejeune, T., & Schaerer, D. 2001, A&A, 366, 538
Lenorzer, A., Mokiem, M. R., de Koter, A., & Puls, J. 2004, A&A, 422, 275
Liseau, R., Lorenzetti, D., Nisini, B., Spinoglio, L., & Moneti, A. 1992, A&A, 265, 577
Martín-Hernández, N. L., Bik, A., Kaper, L., Tielens, A. G. G. M., & Hanson, M. M. 2003, A&A, 405, 175
Martins, F., Schaerer, D., & Hillier, D. J. 2002, A&A, 382, 999
Martins, F., Schaerer, D., Hillier, D. J., & Heydari-Malayeri, M. 2004, A&A, 420, 1087
Mason, B. D., Gies, D. R., Hartkopf, W. I., et al. 1998, AJ, 115, 821
Massey, P., Parker, J. W., & Garmany, C. D. 1989, AJ, 98, 1305
Murphy, D. C., & May, J. 1991, A&A, 247, 202
Penny, L. R. 1996, ApJ, 463, 737
Preibisch, T., Balega, Y., Hofmann, K., Weigelt, G., & Zinnecker, H. 1999, New Astron., 4, 531
Puls, J., Kudritzki, R.-P., Herrero, A., et al. 1996, A&A, 305, 171
Smith, L. J., Norris, R. P. F., & Crowther, P. A. 2002, MNRAS, 337, 1309
Sung, H., Bessell, M. S., & Lee, S. 1998, AJ, 115, 734
Thé, P. S., Bakker, R., & Antalova, A. 1980, A&AS, 41, 93
van Buren, D., Mac Low, M., Wood, D. O. S., & Churchwell, E. 1990, ApJ, 353, 570
Walsh, A. J., Burton, M. G., Hyland, A. R., & Robinson, G. 1998, MNRAS, 301, 640
Watson, A. M., & Hanson, M. M. 1997, ApJ, 490, L165
Wood, D. O. S., & Churchwell, E. 1989a, ApJ, 340, 265
Wood, D. O. S., & Churchwell, E. 1989b, ApJS, 69, 831
Zinnecker, H. 2003, in A massive star odyssey: from main sequence to supernova., IAU Symp., 212, 80

Online Material

Table 6. Identification of the OB stars and observing log. Column 1: associated IRAS pointsource, Col. 2: source number, taken from Kaper et al. (2005), Col. 3: class of object; OB: OB stars; YSO: candidate massive YSO; NEB: nebular UCHII radio source counterpart; LT: late-type stars, Col. 4: total integration time, Col. 5: obtained signal-to-noise ratio, Col. 6: observed standard star used to remove the telluric lines, Cols. 7 and 8: K and $J-K$ values taken from Kaper et al. (2005) †: this source is slightly extended and no point source photometry was possible.

IRAS	nr	Class	Exp	*S/N*	Standard star	K	$J-K$
06058+2138	221	YSO	600	122	HD 43726 (A1V)	10.7 ± 0.03	3.8 ± 0.11
06058+2138	227	YSO	600	148	HD 43726 (A1V)	10.7 ± 0.03	>7.0
06058+2138	534	OB	600	125	HD 43726 (A1V)	10.4 ± 0.02	1.3 ± 0.04
06061+2151	153	LT	960	110	HD 43726 (A1V)	11.69 ± 0.04	4.64 ± 0.26
06061+2151	674A	OB	960	161	HD 43726 (A1V)	11.8 ± 0.04	2.0 ± 0.09
06061+2151	676	YSO	960	30	HD 43726 (A1V)	13.3 ± 0.08	4.2 ± 0.5
06084−0611	114	YSO	960	200	HD 43726 (A1V)	9.3 ± 0.01	4.7 ± 0.08
06084−0611	118	YSO	960	184	HD 43726 (A1V)	10.8 ± 0.03	4.2 ± 0.14
06412−0105	94	LT	960	200	HD 48829 (B9V)	10.09 ± 0.02	0.95 ± 0.03
06412−0105	121	YSO	960	108	HD 48829 (B9V)	10.2 ± 0.02	1.8 ± 0.04
06567−0355	122	LT	960	170	HD 48829 (B9V)	11.22 ± 0.03	4.38 ± 0.17
06567−0355	257	LT	960	140	HD 48829 (B9V)	13.00 ± 0.07	1.74 ± 0.14
06567−0355	557	OB	960	141	HD 48829 (B9V)	11.6 ± 0.04	2.6 ± 0.10
06567−0355	589	OB	960	156	HD 48829 (B9V)	10.4 ± 0.02	3.2 ± 0.07
07299−1651	43	YSO	960	145	HD 65674 (A0V)	9.4 ± 0.01	4.7 ± 0.09
07299−1651	314	YSO	960	90	HD 65674 (A0V)	11.5 ± 0.03	>6.0
07299−1651	533	LT	960	170	HD 65674 (A0V)	11.6 ± 0.04	3.34 ± 0.13
07299−1651	598	YSO	960	131	HD 65674 (A0V)	11.2 ± 0.03	1.6 ± 0.06
07299−1651	618	YSO	960	175	HD 65674 (A0V)	9.4 ± 0.01	4.8 ± 0.09
08563−4711	314	OB	600	189	HD 80998 (B8V)	8.9 ± 0.01	1.4 ± 0.02
08563−4711	317	OB	600	161	HD 80998 (B8V)	10.0 ± 0.02	2.3 ± 0.04
08576−4334	179	OB	600	134	HD 80055 (A0V)	9.6 ± 0.01	1.9 ± 0.03
08576−4334	201	LT	600	115	HD 80055 (A0V)	9.61 ± 0.02	2.70 ± 0.04
08576−4334	225	LT	600	230	HD 80055 (A0V)	9.45 ± 0.01	3.26 ± 0.05
08576−4334	292	YSO	960	107	HD 80055 (A0V)	9.4 ± 0.01	2.4 ± 0.03
08576−4334	408	YSO	600	173	HD 80055 (A0V)	7.3 ± 0.03	3.1 ± 0.02
08576−4334	413	OB	600	255	HD 80055 (A0V)	7.5 ± 0.01	1.8 ± 0.01
08576−4334	461	OB	600	63	HD 80055 (A0V)	12.7 ± 0.06	1.7 ± 0.11
08576−4334	462	OB	600	183	HD 80055 (A0V)	7.0 ± 0.01	1.8 ± 0.01
09002−4732	697	OB	960	160	HD 80998 (B8V)	10.7 ± 0.03	5.4 ± 0.22
09002−4732	738	LT	960	30	HD 80998 (B8V)	13.72 ± 0.11	3.35 ± 0.37
10049−5657	261	LT	600	120	HD 91373 (A0V)	9.33 ± 0.01	2.11 ± 0.03
10049−5657	324	OB	600	109	HD 91373 (A0V)	10.5 ± 0.02	2.8 ± 0.06
10049−5657	411	OB	600	84	HD 91373 (A0V)	11.7 ± 0.04	2.9 ± 0.11
11097−6102	693	YSO	600	160	HD 102152 (A0V)	9.6 ± 0.01	3.4 ± 0.04
11097−6102	1122	OB	960	179	HD 102152 (A0V)	10.5 ± 0.02	2.4 ± 0.05
11097−6102	1218	YSO	600	183	HD 102152 (A0V)	8.4 ± 0.01	5.6 ± 0.09
12073−6233	1016	LT	1200	134	HD 110062 (B9V)	7.96 ± 0.01	8.89 ± 0.01
12073−6233	1974	OB	1200	168	HD 110062 (B9V)	10.7 ± 0.03	2.3 ± 0.05
12073−6233	2851	OB	1200	96	HD 110062 (B9V)	10.7 ± 0.03	2.5 ± 0.06
15408−5356	1410	OB	600	140	HD 137251 (A2V)	8.6 ± 0.01	2.2 ± 0.02
15408−5356	1454	OB	600	158	HD 137251 (A2V)	9.3 ± 0.01	2.1 ± 0.03
15411−5352	462	LT	600	100	HD 137251 (A2V)	8.14 ± 0.01	6.95 ± 0.13
15411−5352	1955	YSO	600	188	HD 137251 (A2V)	7.9 ± 0.01	4.3 ± 0.03
15502−5302	2960	OB	960	62	HD 137251 (A2V)	13.0 ± 0.08	2.6 ± 0.19
15502−5302	3167	OB	960	106	HD 137251 (A2V)	11.8 ± 0.04	1.6 ± 0.19
16128−5109	1182	LT	960	180	HD 150628 (A0V)	10.14 ± 0.02	5.88 ± 0.20
16164−5046	1542	OB	960	119	HD 150628 (A0V)	11.7 ± 0.04	2.0 ± 0.08
16164−5046	3636	YSO	960	137	HD 150628 (A0V)	9.5 ± 0.02	≥8.1
16177−5018	271	OB	960	40	HD 150628 (A0V)	11.8 ± 0.04	3.4 ± 0.14

Table 6. continued.

IRAS	nr	Class	Exp	*S/N*	Standard star	*K*	*J* − *K*
16177−5018	405	OB	960	131	HD 150628 (A0V)	10.8 ± 0.03	≥6.7
16177−5018	1020	OB	960	98	HD 150628 (A0V)	11.9 ± 0.04	4.7 ± 0.27
16177−5018	2239	LT	960	60	HD 150628 (A0V)	8.77 ± 0.01	2.53 ± 0.02
16571−4029	820	OB	960	124	HD 158684 (A0V)	9.3 ± 0.01	2.6 ± 0.03
16571−4029	1281	YSO	960	132	HD 158684 (A0V)	9.3 ± 0.01	2.5 ± 0.06
16571−4029	1610	OB	960	132	HD 158684 (A0V)	11.0 ± 0.03	2.5 ± 0.07
17136−3617	447	LT	960	100	HD 161759 (A0V)	9.45 ± 0.01	7.81 ± 0.40
17136−3617	649	YSO	960	191	HD 161759 (A0V)	9.5 ± 0.01	3.8 ± 0.06
17136−3617	712	LT	960	170	HD 161759 (A0V)	8.55 ± 0.01	6.05 ± 0.11
17149−3916	792	LT	600	70	HD 161759 (A0V)	8.68 ± 0.01	3.39 ± 0.01
17149−3916	895	OB	600	139	HD 161759 (A0V)	8.3 ± 0.01	0.6 ± 0.01
17149−3916	1061	LT	600	30	HD 161759 (A0V)	10.42 ± 0.02	5.47 ± 0.17
17149−3916	3361	LT	600	50	HD 161759 (A0V)	12.87 ± 0.06	1.50 ± 0.10
17175−3544	59	OB	960	166	HD 161759 (AOV)	11.5 ± 0.03	6.3 ± 0.5
17258−3637	378	OB	960	141	HD 161759 (A0V)	10.2 ± 0.02	3.4 ± 0.06
17258−3637	593	YSO	960	200	HD 161759 (A0V)	9.6 ± 0.01	5.5 ± 0.17
17258−3637	1558	OB	960	17	HD 161759 (A0V)	10.7 ± 0.02	1.9 ± 0.04
17423−2855	3102	OB	960	113	HD 166131 (B8V)	9.9 ± 0.02	5.3 ± 0.13
17423−2855	3130	LT	960	60	HD 166131 (B8V)	10.81 ± 0.03	>6.8
17423−2855	6909	LT	960	80	HD 166131 (B8V)	9.47 ± 0.01	15.89 ± 0.18
17574−2403	930	LT	960	80	HD 171572 (B9V)	9.89 ± 0.02	>7.8
17574−2403	3471	LT	960	100	HD 171572 (B9V)	10.53 ± 0.02	1.27 ± 0.04
17574−2403	xx[†]	NEB	960	32	HD 171572 (B9V)	–	–
18006−2422	766	YSO	600	146	HD 171808 (A0V)	9.4 ± 0.01	2.8 ± 0.04
18006−2422	770	OB	600	131	HD 171808 (A0V)	7.3 ± 0.01	0.9 ± 0.01
18006−2422	702	LT	600	102	HD 171808 (A0V)	9.93 ± 0.02	4.29 ± 0.08
18006−2422	1134	LT	600	150	HD 171808 (A0V)	9.04 ± 0.04	3.49 ± 0.04
18006−2422	2035	NEB	600	88	HD 171808 (A0V)	11.4 ± 0.04	1.8 ± 0.07
18060−2005	719	LT	600	70	HD 171808 (A0V)	9.49 ± 0.01	5.54 ± 0.13
18060−2005	1073	LT	600	80	HD 171808 (A0V)	10.46 ± 0.02	5.26 ± 0.18
18060−2005	1733	OB	600	100	HD 171808 (A0V)	9.0 ± 0.01	2.9 ± 0.03
18060−2005	2481	OB	960	75	HD 171808 (A0V)	11.1 ± 0.03	3.5 ± 0.11
18449−0158	319	OB	960	93	HD 181690 (B9V)	10.8 ± 0.03	2.4 ± 0.06
18449−0158	335	OB	960	159	HD 181690 (B9V)	8.5 ± 0.01	7.0 ± 0.17
18449−0158	1493	LT	960	80	HD 181690 (B9V)	10.71 ± 0.03	2.37 ± 0.06
18507+0110	262	OB	960	190	HD 181690 (B9V)	9.4 ± 0.01	4.3 ± 0.07
18507+0110	248	YSO	960	153	HD 181690 (B9V)	10.3 ± 0.02	5.4 ± 0.18
18507+0110	373	OB	960	70	HD 181690 (B9V)	12.3 ± 0.05	5.4 ± 0.49
18507+0110	389	OB	960	90	HD 181690 (B9V)	11.3 ± 0.03	3.8 ± 0.14
18592+0108	1035	LT	960	120	HD 181690 (B9V)	11.31 ± 0.03	4.08 ± 0.14
18592+0108	1051	LT	960	130	HD 181690 (B9V)	11.29 ± 0.03	5.00 ± 0.21
18592+0108	1555	NEB	960	40	HD 181690 (B9V)	12.6 ± 0.05	>5.1
19078+0901	185	LT	960	90	HD 186549 (B9V)	10.69 ± 0.02	3.74 ± 0.10
19078+0901	438	LT	960	110	HD 186549 (B9V)	11.63 ± 0.04	4.10 ± 0.19
19078+0901	549	LT	960	130	HD 186549 (B9V)	11.88 ± 0.04	5.01 ± 0.33
19078+0901	647	OB	960	65	HD 186549 (B9V)	13.2 ± 0.07	4.4 ± 0.5
19078+0901	670	LT	960	80	HD 186549 (B9V)	10.11 ± 0.02	2.17 ± 0.04
19078+0901	1202	LT	960	120	HD 186549 (B9V)	10.31 ± 0.02	3.75 ± 0.09
19078+0901	2070	NEB	960	32	HD 186549 (B9V)	13.5 ± 0.07	>4.2
19078+0901	2224	NEB	960	33	HD 186549 (B9V)	13.1 ± 0.07	>4.6
19111+1048	207	LT	960	70	HD 186549 (B9V)	11.23 ± 0.05	2.77 ± 0.12
19111+1048	1149	LT	960	70	HD 186549 (B9V)	11.15 ± 0.05	1.89 ± 0.08